Correlation of fluvial terraces and temporal steady-state incision on the onshore Makran accretionary wedge in southeastern Iran: Insight from channel profiles and ^{10}Be exposure dating of strath terraces

Negar Haghipour[1,†], Jean-Pierre Burg[1], Susan Ivy-Ochs[2], Irena Hajdas[2], Peter Kubik[2], and Marcus Christl[2]
[1]*Geological Institute, ETH Zurich, Sonneggstrasse 5, CH-8092 Zurich, Switzerland*
[2]*Laboratory of Ion Beam Physics, ETH Zurich, Schafmattstrasse 20, CH-8093 Zurich, Switzerland*

ABSTRACT

We describe and summarize the geomorphology of fluvial terraces along the four major rivers draining the central, onshore Makran accretionary wedge in Iran, and describe uplifted marine terraces on the coast of this region. Thirty-five strath terraces at different sites were dated using in situ–produced cosmogenic ^{10}Be concentrations from surfaces and depth profiles. These new measurements reveal abandonment ages between ca. 15 and 380 ka. The age distribution allows determining the chronology of terrace levels and establishing regional correlations between two major regional levels. The geographically widespread correspondence suggests that these two levels result from a regional, climatically driven force. Systematic dating also provides evidence for time and spatial variations in incision rate, which enables distinguishing between a regionally uniform incision rate of 0.3–0.4 mm/a and higher local incision and/or uplift (~0.8 mm/a) rates. These spatial changes are consistent with where localized tectonic activity is recognized in the field. We also dated, using ^{14}C in shells, four uplifted marine terraces on the coast of the study area. Comparing incision rates derived from strath terraces (0.3 mm/a) with published uplift estimates from marine terraces (0.2 mm/a) reveals that fluvial rivers responded to a regional, long-term incision and surface uplift pattern. This rate reflects the tectonically steady state of the wedge on a regional scale. Locally high incision rates delineate active faults and folds, indicating that perfect steady state is unlikely on short length scales.

[†]E-mail: negar.haghipour@erdw.ethz.ch.

INTRODUCTION

The spatial and temporal distribution of deformation is a central issue to characterizing the bulk, natural rheology of major tectonic units. This information is in turn needed to refine numerical models of geodynamic processes. In attempting this, tectonic geomorphology has proven to be a very efficient approach, revealing the direct response of surface processes to tectonic activity (e.g., Burbank and Anderson, 2001; Bull, 2009). Many applications in active mountain regions have established the relevance of such an approach (e.g., Hartshorn et al., 2002; Montgomery and Brandon, 2002; Friend et al., 2009). The concept of equilibrium between surface slope, basal slope, basal friction, and internal friction of orogenic wedges has often been applied to seismic and geological profiles of fold-and-thrust belts (e.g., Spence et al., 1991; DeCelles and Mitra, 1995; Bilotti and Shaw, 2005). One little-explored topic is the interplay between surface processes and the dynamic evolution of such belts over wide areas (e.g., Storti and McClay, 1995; Simpson, 2010). Given that fluvial terraces are preserved in all of the main Makran river valleys (Iran), they are good targets for regional correlation and therefore long-term incision/uplift studies.

Incision and aggradation in fluvial networks are dictated by three main factors: (1) base level change (Blum and Törnqvist, 2000; Blum et al., 2001), (2) climate oscillations (Molnar et al., 1994), and (3) tectonic activity (e.g., Seeber and Gornitz, 1983; Burbank et al., 1994). However, because these factors generally interact in a complex manner, it remains difficult to decipher their respective roles (Wegmann and Pazzaglia, 2009).

In this work, we extend the techniques of tectonic geomorphology to refine our understanding of the surface behavior of the accretionary wedge of Makran in southern Iran. Our motivation is to offer a large-scale, quantitative morphotectonic study covering a wide subaerial wedge surface. This study reports and compares geochronologic data complementing field observations from four adjacent catchments that drain much of the onshore Makran accretionary wedge. We used dated strath terraces as geomorphic reference markers (Lavé and Avouac, 2001; Pazzaglia and Brandon, 2001; Pazzaglia, 2013) in combination with river longitudinal profiles to extract and determine local surface uplift and/or incision (Snyder et al., 2000; Whipple et al., 2000; Kirby and Whipple, 2001; Whipple, 2004). Results permit us to identify the regional correlations and develop a robust interpretation of the landscape response to tectonic and climate changes (e.g., Van den Berg and van Hoof, 2001). The geomorphological record demonstrates two length scales of time-averaged uplift and/or incision rates linked to distributed and localized tectonic deformation. We foresee that the measured vertical velocities can be transformed into a full accretion rate and are key to the internal dynamics of the wedge on a different time scale than denudation rates derived from low-temperature geochronology (e.g., Brandon et al., 1998; Willett et al., 2003).

SETTING

Geological Setting

The Makran accretionary wedge occupies the subduction zone between the Arabian plate to the south and the Eurasian plate to the north (Fig. 1). This north-dipping subduction is thought to have begun in the Late Cretaceous (Farhoudi and Karig, 1977; McCall, 1997). The wedge is the largest exposed on Earth, extending more than 1000 km from the Minab

GSA Bulletin; March/April 2015; v. 127; no. 3/4; p. 560–583; doi: 10.1130/B31048.1; 15 figures; 3 tables; published online 22 October 2014.

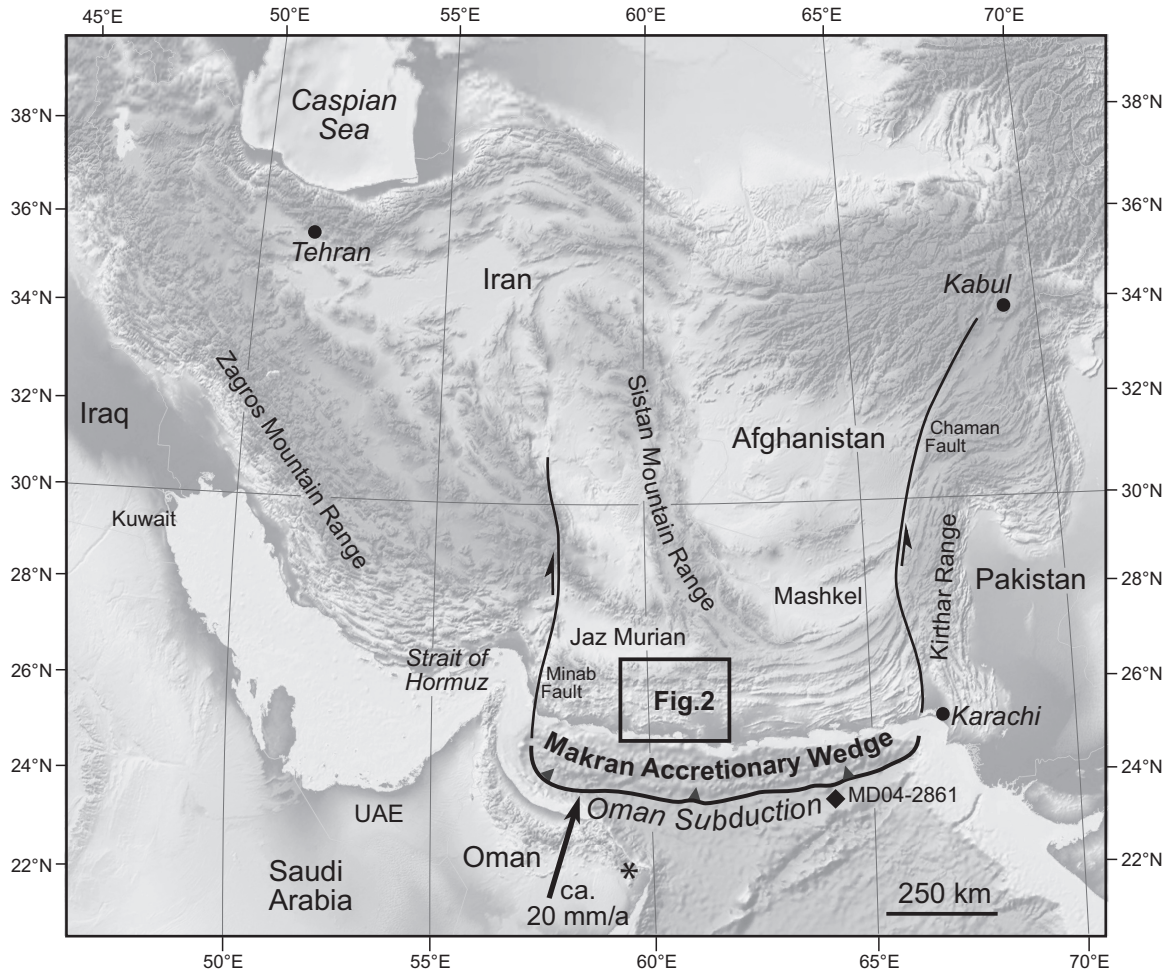

Figure 1. Tectonic setting of the Makran subduction zone. The convergence arrow is the GPS convergence rate between Arabia and stable Eurasia, after Vernant et al. (2004). StarHoti cave with speleothems studied by Burns et al. (1998); diamond—core studied by Clemens and Prell (2003). UAE—United Arab Emirates. Background: shaded relief map ETOPO1 (http://www.ngdc.noaa.gov/mgg/global/relief/ETOPO1).

fault zone to the west, in Iran, to the Chaman fault zone to the east, in Pakistan (Fig. 1). The high incoming sediment thickness (~7 km) and a low taper angle of ~3° (Davis et al., 1983) are exceptional characteristics of Makran wedge. Accepting the classical Coulomb wedge theory (Davis et al., 1983), the small taper suggests either a weak basal décollement or a high internal strength. In any case, the wedge should grow in a self-similar manner, combining frontal accretion, tectonic underplating, and normal faulting (Fig. 2), so that its long-term bulk topography rises uniformly and steadily (Dahlen, 1990).

The studied part of Makran covers an area of the exposed accretionary wedge ~150 km across and 250 km trench parallel in southeastern Iran, away from the lateral Minab and Chaman transform boundaries. Four tectonostratigraphic units separated by major thrust faults have been distinguished in the bedrock of the study area (Fig. 2). From the north to the south, i.e., from the structural top to bottom, these units are: North Makran, Inner Makran, Outer Makran, and Coastal Makran (Dolati, 2010; Burg et al., 2012). The main fault system is composed of flat-and-ramp thrusts, which reflect a thin-skinned fold-and-thrust belt over blind décollement surfaces (Burg et al., 2012). The Bashakerd thrust is the tectonic boundary between North Makran, which exposes ophiolite-bearing "colored mélanges" and deep-sea sediments and volcanics (McCall, 2002; Dolati, 2010), and the turbidite-dominated Inner Makran. The Inner, Outer, and Coastal Makran units include Eocene to recent sediments deformed in the fold-and-thrust belt. Folding and thrusting were active before, and reactivated after, the emplacement of a Tortonian (ca. 10 Ma) olistostrome (Burg et al., 2008). Folding and thrusting caused middle Miocene to Pliocene growth structures. Most of the deformation was then shifted to the present-day submarine wedge, perhaps as a consequence of the load brought by the olistostrome (Smit et al., 2010). However, deformation did not stop onshore, so that some of the studied terraces have been folded in the last 120 k.y. (Haghipour et al., 2012). We further constrain the Quaternary deformation of the Makran wedge with this study, which is focused upon surface uplift and subsequent fluvial incision rate, which we use as a proxy of the internal deformation of the wedge. The only uplift rates reported for Makran were derived from marine terraces dated with uranium series and ^{14}C (Falcon, 1975; Vita-Finzi, 1975; Page et al., 1979; Snead, 1992). Mean uplift of the coast was estimated at 0.2 mm/a in the Pleistocene and 2 mm/a in the Holocene.

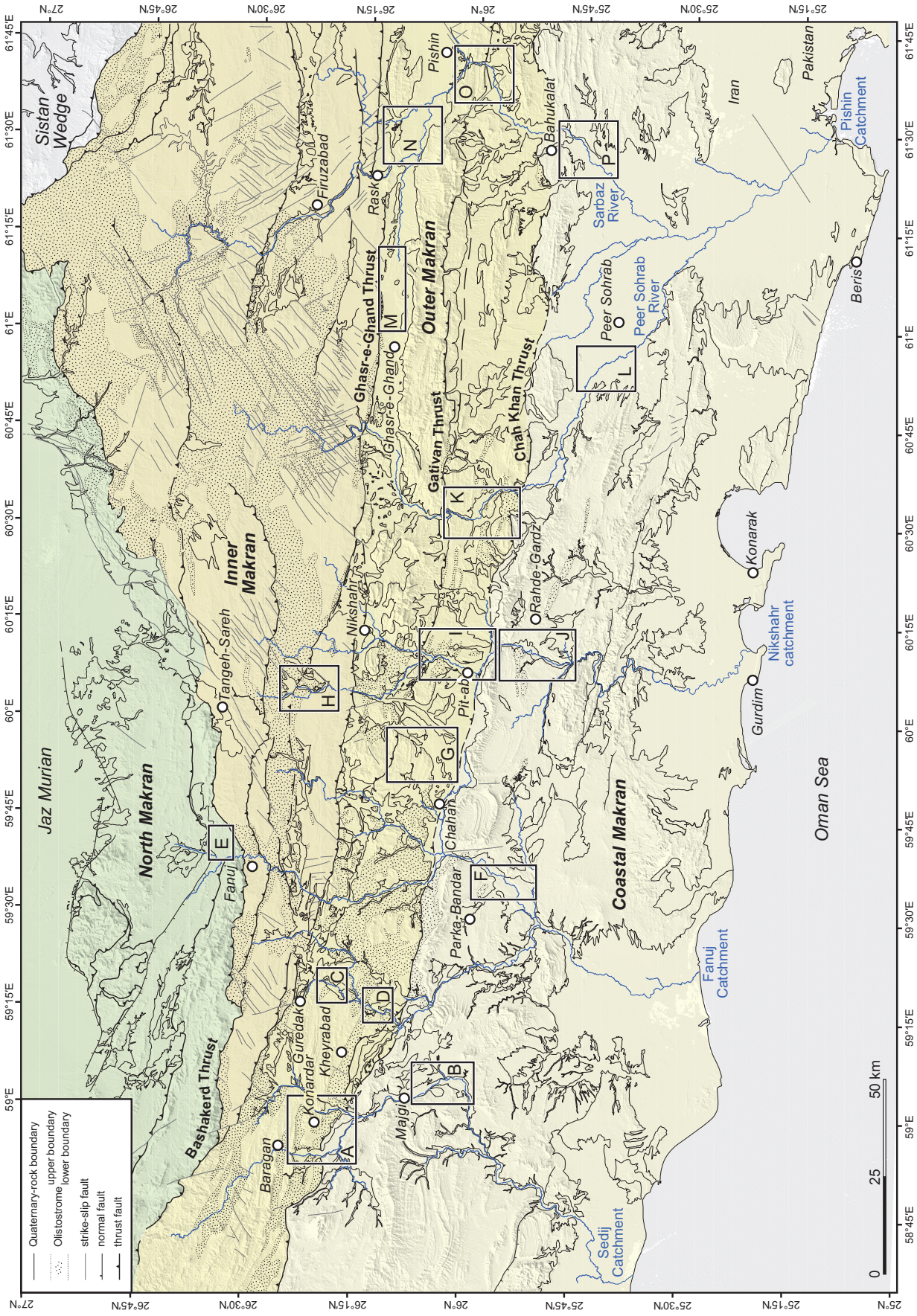

Figure 2. Simplified geological map of the central Makran fold-and-thrust belt in Iran (extended from Burg et al., 2012). The four lithotectonic units are: North Makran of mostly Cretaceous rocks (green); Inner Makran of mostly Eocene to middle Miocene rocks (brown); Outer Makran of mostly upper Oligocene to middle Miocene rocks (yellow); and Coastal Makran of mostly upper Miocene and Plio-Pleistocene sediments (light beige). Lettered boxes indicate the studied sites described in text. White circles are main cities and villages.

Seismicity—Active Tectonics

Geodetic data at the longitude of the Gulf of Oman document a roughly north-south convergence rate of ~2 cm/a (Vernant et al., 2004; Masson et al., 2005). Compared to other convergence zones (e.g., Tonga subduction zone, 16 cm/a [Bevis et al., 1995]; Sumatra subduction zone, 6.5 cm/a [Gahalaut and Catherine, 2006]), Makran is a slow subduction zone, often compared to the Cascadia subduction zone (3.5 cm/a; Wong, 2005). Although the region has experienced large earthquakes such as the M_w 8.1, A.D. 1945 event (Jackson and McKenzie, 1984; Byrne et al., 1992), the present-day Makran, like Cascadia, is in an interseismic interval. Byrne et al., 1992 suggested that high pore pressure of unconsolidated and water-saturated sediments causes this low seismicity. The low taper would result from these overpressured, low-friction sediments (Smit et al., 2010). Mud volcanoes along the Iranian and Pakistani coasts of Makran substantiate the concept of overpressured shale layers at depth.

Climate Setting

The frequency, direction, and timing of Quaternary climate changes in Iran are sparsely documented, compared to the extensive literature from other parts of the world. Evidence of Pleistocene and Holocene climate fluctuations in Iran is based on several sources, such as lake sediment (e.g., van Zeist and Wright, 1963; Djamali et al., 2008), glacial moraines (e.g., Kuhle, 2008; Kehl, 2009), alluvial sediments (Vita-Finzi, 1969), and fluvial and marine terraces (Degens and Paluska, 1979; Regard et al., 2006). The present climate of Makran is arid to semi-arid with a mean annual precipitation of 113 mm/a. The dryness is caused by northeasterly winds that transport mainly dry air masses. It is further enhanced by the mountain ranges in the north (Alborz) and southwest (Zagros), which prevent northwesterly and westerly depressions from the Caspian and Mediterranean Seas from entering the Iranian Plateau (Kehl, 2009). Two main sources of monsoon winds, the summer and winter monsoons, govern the modern climate around the Arabian Sea (Fig. 3). Marine sediments from the Makran margin show that the northern Arabian Sea is controlled by a southwest monsoon rather than by a northeast monsoon (Caley et al., 2011). The paleoclimate record based on speleothems from Hoti cave (northern Oman; Fig. 1; Burns et al., 1998) provides information on two periods of wetness: (1) 9.7–6.2 ka, and (2) the last interglacial (marine isotope stage [MIS] 5). Fluid inclusions in speleothems from the same cave record continental pluvial periods at 6–10, 78–82, 120–135, 180–200, and 300–330 ka (Fleitmann et al., 2003). The present-day main

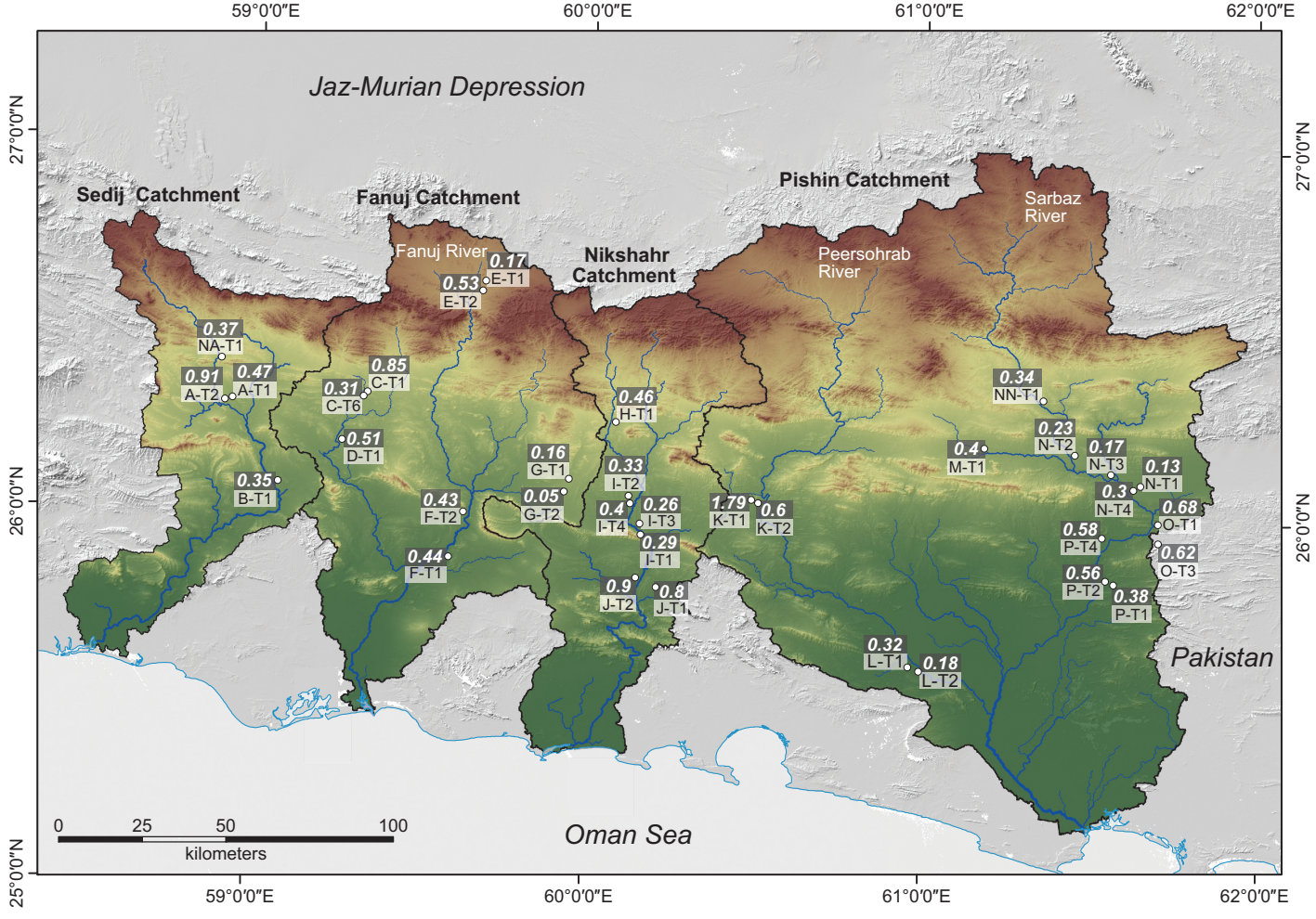

Figure 3. Shaded relief map (ASTER GDEM [Global Digital Elevation Map], version 1, NASA) showing the studied catchments in Iran. Dark boxes with italic white numbers indicate local incision rates (mm/a). Light boxes with black numbers are sample numbers reported in Tables 1 and 2. White dots are sample locations.

rain season is from December to February; water discharge in the four studied catchments is mainly derived from heavy and short winter rainfalls that produce flash floods and coastal-plain inundation.

METHODS

Field Observation and Surveying

Fluvial terraces of the Makran valleys had not been studied beyond reconnaissance surveys (Falcon, 1975; McCall and Kidd, 1982). Very recent studies (Haghipour et al., 2012; Kober et al., 2013) provide few age constraints, but only on the local or single-catchment scale. Most of the studies on Quaternary deposits in eastern and central Iran are limited to the Holocene (e.g., Walker and Fattahi, 2011). We mapped fluvial terraces parallel to the main trunks and main tributaries of four contiguous catchments flowing southward, nearly perpendicular to the strike of the major geological structures (Fig. 2), down to the Oman Sea. Mapping was based on aerial photographs (scale 1:50,000) using ERDAS IMAGINE V11 software, satellite images, and an ASTER digital elevation model (G-DEM) with 1 arcsec (~30 × 30 m) resolution. Terraces were mapped and classified in sequence according to their relative elevation with respect to the local stream, in increasing order from T1, the locally highest level. Field verification focused on important and critical geomorphologic features identified on remote images. The river segments between these critical points were surveyed in a less detailed manner, unless unexpected features were discovered. A handled GPS (Garmin Vista Cx) with barometric altimeter was systematically used to measure the elevation of strath terraces and modern channel beds. We admit a 4 m uncertainty for the absolute measured elevations. The thickness of the alluvial cover was measured with a tape. In places where the alluvial cover is >3 m, the strath elevation measured by GPS was corrected for the thickness of the alluvial cover. Fieldwork priorities focused upon identifying the most reliable sampling sites for dating and spatial correlation. Topographic shielding of ^{10}Be sample collection sites was measured with high-precision compass and clinometer (1° error for both measurements). Both aggradational (fill) and degradational (strath) terraces occur along the four river networks. Although strath terraces are dominant, we also dated fill terraces for a complete record of river incision and aggradation. The description of sampled surfaces, topographic shielding, and GPS positions is given in Table 1.

Channel Steepness Indices

Under some simplifications, elevation versus distance profiles of rivers in dynamic equilibrium with their environment (i.e., the amount of sediment they can transport away balances the amount of material their drainage areas deliver) tend to follow a smooth, concave-upward power-law function (Hack, 1957; Smith et al., 2000). Flint's law expresses this empirical assertion, where the local channel slope (S) is inversely proportional to the upstream drainage area (A) of the river to the power of an exponent θ called the concavity index (Flint, 1974):

$$S = K_S A^{-\theta}, \quad (1)$$

where K_S is the channel steepness index. θ is a critical exponent because it defines the shape of the length profile of detachment-limited channels, those where vertical abrasion and plucking can equal (or overcome) tectonic uplift of the bedrock or base-level fall (Hancock et al., 1998; Whipple and Tucker, 1999). Best-fit values of θ = 0.25–0.6 represent long-term equilibrium between erosion and rock uplift rates (Whipple and Tucker, 1999; Kirby and Whipple, 2001). The value θ = 0.5 is accepted to be pragmatically realistic in modeling fluvial erosion if climatic conditions and basement erodibility are uniform over the studied drainage system (e.g., Kirby and Whipple, 2001; Tucker and Whipple, 2002; Wobus et al., 2006). Following these predictions and assumptions, the K_S value stands as a convenient index metric to locate tectonic or lithological anomalies (e.g., Merritts and Vincent, 1989). This steepness index, however, does not quantify uplift rates. In practice, one extracts a normalized channel steepness index using a reference concavity θ_{ref} in order to best compare relative changes in nonlinear profiles of different channels (Sklar and Dietrich, 1998; Wobus et al., 2006). The normalized form of Equation 1 is

$$S = K_{Sn} A^{-\theta ref}, \quad (2)$$

in which K_{Sn} is a measure of the rock uplift rate in areas with steady-state landscape (e.g., Snyder et al., 2000; Kirby and Whipple, 2001; Hilley and Arrowsmith, 2008). Applying this equation generates ideal long profiles to which actual river profiles can be paralleled. Deviations between the ideal and actual profiles are diagnostic for dynamic disequilibrium between the river and its environment. Field observations in departing river segments provide keys to decide whether tectonic uplift or subsidence, changes in rock erodibility or base level, climate, or other environmental changes are responsible for profile divergence. For this study, we followed the methodology provided by Wobus et al. (2006) and used a set of Matlab and ArcGIS scripts (http://www.geomorphtools.org) to calculate K_{Sn} for the studied river networks.

Cosmogenic Nuclide Dating and Sampling

The lithological content of the studied fluvial terraces (essentially mixed pebbles and coarse gravel) and the lack of datable and correlatable material such as sand or silt lenses, ash layers, and organic matter restricted dating possibilities to terrestrial cosmogenic nuclides (TCN). We employed the in situ terrestrial ^{10}Be cosmogenic nuclide method because the investigated sites did not offer suitable samples for optically stimulated luminescence. ^{10}Be and ^{26}Al are produced from the interaction of secondary cosmic rays with Si and O in quartz at and near the Earth surface (e.g., Lal, 1991; Gosse and Phillips, 2001). Sampled sites met several conditions. (1) They belong to paired and well-preserved terraces. This precaution is necessary because paired surfaces indicate that the river has not shifted laterally for large distances and therefore had a nearly constant geometry since the studied terraces were formed in the bedrock stream section, whereas unpaired, small terraces may result from local tectonic or autocyclic processes unrelated to regional signals of tectonic and climate forcing. (2) There was no sign of bioturbation (including human activity) or any surface disturbance such as colluvial deposits. (3) We chose wide, planar terraces whose surface shows the least evidence for erosion, with minimal surface (tread) relief (Figs. 4A and 4B), which could affect TCN ages (e.g., Matmon et al., 2009). (4) The sampled terrace profiles contain rounded, tiled clasts typifying their fluvial environment.

We dated 35 sites along six rivers of the four investigated catchments (Fig. 3) using the amalgamation method (Anderson et al., 1996; Repka et al., 1997). Dating the exposed surface of single clasts is an alternative method, taking the youngest absolute age as the closest estimate of the age of the depositional surface (Frankel et al., 2007; Vassallo et al., 2011). However, ^{10}Be measurements of single clast surfaces may strongly vary from clast to clast, depending on several geologic factors such as erosion and fluvial transport (e.g., Owen et al., 2011). Consequently, the inferred age may be older or younger than the actual time of landform deposition, as much as for the amalgamation approach (Schmidt et al., 2011; Ivy-Ochs et al., 2012). In any case, the small, few-centimeters size of clasts in Makran terraces is inappropriate for single clast analysis.

TABLE 1. SAMPLE INFORMATION AND MEASURED ^{10}Be CONCENTRATION

Sample number	Local terrace name	Latitude (N)	Longitude (E)	Elevation (m above sea level)	Depth (cm)	^{10}Be, blank corrected (10^5 atoms/g)	± (10^5 atoms/g)	Topographic shielding	Site
Sedij catchment									
Q-Mak-10-36	A-T1	26.3191	58.8900	411	0	4.480	0.20	1	A
Q-Mak-10-37	A-T2	26.3161	58.8838	388	0	1.134	0.06	1	A
Q-Mak-10-38	NA-T2	26.4058	58.8902	471	0	0.998	0.05	1	A
Q-Mak-09-41	B-T1	26.0850	59.0622	241	0	4.373	0.19	1	B
Q-Mak-09-43	B-mch	26.0908	59.0443	199	0	0.961	0.09	0	B
Q-Mak-11-25	A-mch	26.3449	58.8822	380	0	0.746	0.05	0	A
Fanuj catchment									
Q-Mak-09-49	C-T1	26.3188	59.3258	417	0	2.940	0.14	1	C
Q-Mak-09-45	C-T6	26.3130	59.3202	373	0	0.636	0.07	1	C
Q-Mak-10-40	D-T1	26.1966	59.2669	300	0	3.947	0.17	1	D
Q-Mak-09-56	E-T1	26.6088	59.7636	941	0	8.550	0.33	1	E
Q-Mak-09-57	E-T2	26.6089	59.7615	931	0	1.120	0.06	1	E
Q-Mak-09-10	F-T2	25.9817	59.6371	180	0	2.798	0.33	1	F
Q-Mak-11-23	F-T1	25.8836	59.5755	130	0	3.488	0.11	1	F
Q-Mak-10-44	G-T1	26.1593	60.0249	464	0	8.644	0.20	1	G
Q-Mak-10-45	G-T2	26.1114	59.9837	369	0	2.649	0.10	1	G
Q-Mak-09-44	C-mch	26.3125	59.3188	370	0	0.541	0.05	0	C
Q-Mak-11-24	F-mch	25.8912	59.5748	107	0	0.520	0.05	0	F
Nikshahr catchment									
Q-Mak-10-56	I-T4	26.0330	60.1366	273	0	0.949	0.04	1	I
Q-Mak-10-51	Depth profile	26.0330	60.1366	273	20 ± 10	0.710	0.03	–	I
Q-Mak-10-53	Depth profile	26.0330	60.1366	273	50 ± 10	0.416	0.03	–	I
Q-Mak-10-54	Depth profile	26.0330	60.1366	273	140 ± 10	0.420	0.05	–	I
Q-Mak-10-55	Depth profile	26.0330	60.1366	273	180 ± 10	0.576	0.06	–	I
Q-Mak-11-21	I-T1	25.9975	60.1438	281	0	5.858	0.20	1	I
Q-Mak-11-15	I-T2	26.0425	60.1380	302	0	3.993	0.18	1	I
Q-Mak-11-13	I-T3	25.9621	60.1624	220	0	1.835	0.07	–	I
Q-Mak-11-12	H-T1	26.3707	60.1131	759	0	6.966	0.33	1	H
Q-Mak-10-28	J-T1	25.8350	60.1813	240	0	5.801	0.20	1	J
Q-Mak-10-31	J-T3	25.8413	60.1627	144	0	6.966	0.33	1	J
Q-Mak-10-50	J-mch1	25.8327	60.1657	133	0	0.570	0.04	–	J
Q-Mak-11-16	J-mch2	26.0320	60.1399	267	0	1.280	0.08	–	J
Q-Mak-11-14	I-mch	25.8491	60.1686	144	0	1.949	0.07	0	I
Pishin catchment									
Q-Mak-11-01	P-T1	25.9336	61.5513	135	0	3.988	0.15	1	P
Q-Mak-11-02	P-T2	25.9341	61.5477	116	0	1.376	0.07	1	P
Q-Mak-09-62	O-T1	25.9824	61.7008	265	0	7.290	0.19	1	O
Q-Mak-09-32	O-T3	25.9641	61.6816	209	0	4.033	0.10	1	O
Q-Mak-10-22	O-T4	25.9543	61.5543	117	0	1.038	0.09	1	O
Q-Mak-10-19	N-T1	26.1393	61.5819	321	0	16.300	0.93	1	N
Q-Mak-11-09	N-T2	26.1756	61.4638	391	0	10.245	0.30	1	N
Q-Mak-10-14	N-T3	26.1336	61.5569	283	0	6.182	0.30	1	N
Q-Mak-10-15	Depth profile	26.1336	61.5569	283	40 ± 10	3.514	0.14	0	N
Q-Mak-10-16	Depth profile	26.1336	61.5569	283	80 ± 10	2.748	0.11	0	N
Q-Mak-10-17	Depth profile	26.1336	61.5569	283	120 ± 10	1.837	0.10	0	N
Q-Mak-10-18	Depth profile	26.1336	61.5569	283	190 ± 10	1.672	0.07	0	N
Q-Mak-10-20	N-T4	26.1348	61.5835	290	0	5.400	0.15	1	N
Q-Mak-10-03	NN-T1	26.2973	61.3936	558	0	11.801	0.40	1	NN
Q-Mak-10-23	M-T1	26.1911	61.0767	545	0	7.435	0.28	1	M
Q-Mak-10-46	K-T1	26.0494	60.5197	327	0	2.216	0.08	1	K
Q-Mak-10-47	K-T2	26.0447	60.5247	264	0	1.610	0.06	1	K
Q-Mak-11-18	L-T1	25.7561	60.7930	117	0	6.759	0.74	1	L
Q-Mak-11-19	L-T2	25.7505	60.8163	84	0	4.801	0.14	1	L
Q-Mak-11-11	NN-mch	26.2800	61.4231	444	0	1.540	0.07	0	NN
Q-Mak-11-06	O-mch	25.9911	61.6806	152	0	0.963	0.05	0	O
Q-Mak-11-03	P-mch	25.9340	61.5470	97	0	0.828	0.07	0	P
Q-Mak-11-20	L-mch	25.7600	60.7889	54	0	1.253	0.05	0	L
Q-Mak-10-48	K-mch	26.0458	60.5266	245	0	2.162	0.09	0	K
Marine terrace									
Q-Mak-12-2b	Marine terrace	25.351	60.301	77.000	0.000	2.800	0.09	1	Konarak

Note: All samples analyzed for ^{10}Be/^{9}Be ratio at the ETH Zurich Tandem/Tandy Accelerator Mass Spectrometry facility (Kubik and Christl, 2010). Quoted uncertainties are the 1σ internal error. A mean blank ^{10}Be/^{9}Be = 0.004 × 10^{12} was used for correction. mch—modern channel.

We therefore collected more than 30, equal-size, resident quartz–rich clasts at each sampling site. The gathered clasts were crushed and sieved to a grain size of 0.25–0.7 mm. Purified quartz was physically extracted applying magnetic and/or heavy liquid separation methods and chemically purified using HF 40% (e.g., Kohl and Nishiizumi, 1992; Bierman and Nichols, 2004). A known amount (0.3 mg) of ^{9}Be carrier was added to the pure quartz, which was dissolved in concentrated hydrofluoric 40% (HF) and nitric (HNO_3) acids. To extract $Be(OH)_2$, samples were passed through anion and cation exchange columns along with chemical blanks, following

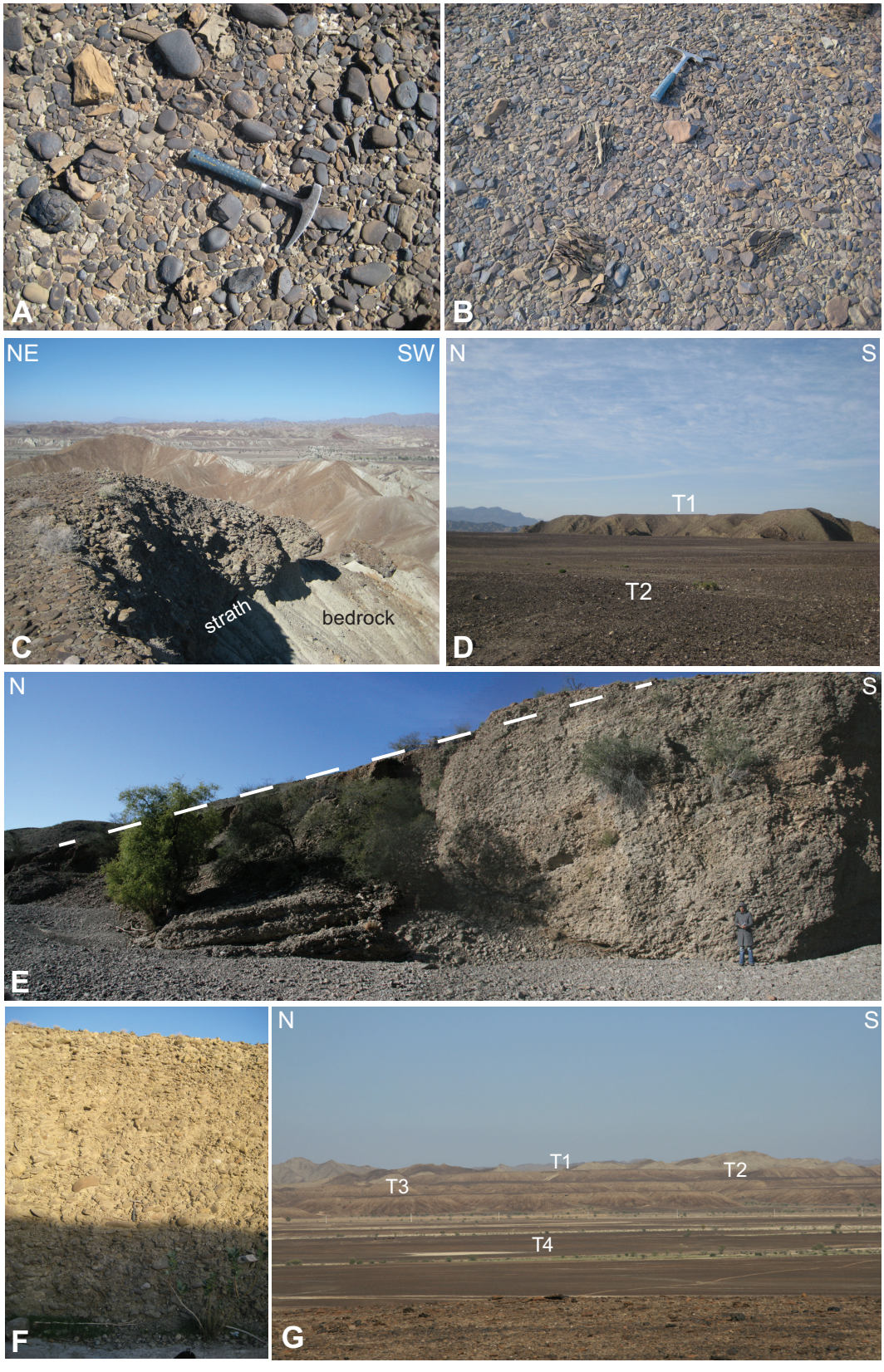

Figure 4. Photographs of fluvial terraces, inland Makran. (A) Sample J-T4 (GPS: (25°50′23.07″N, 60°09′43.50″E). (B) Sample A-T1 (26°19′19.74″N, 58°53′37.88″E). (C) Profile view showing the sharp strath and the clast-supported J-T1 fluvial deposits (26°19′05.11″N, 58°53′46.57″E). The alluvial part is less than 1 m. (D) T1 and T2 levels of strath terraces along Guredak River in the Fanuj catchment (25°50′20.80″N, 60°11′03.90″E). The length of T1 is about 100 m. (E) Tilted fill terrace along Sarbaz River (26°11′48.00″N, 59°16′01.90″E). (F) 10-m-thick fluvial fill along Sarbaz River (26°07′34.61″N, 61°35′08.86″E). (G) T1 to T4 strath terraces along Sarbaz River (25°58′26.66″N, 61°40′57.48″E).

the preparation procedure presented by Ochs and Ivy-Ochs (1997).

The analyses were carried out at the ETH Zurich Tandem and Tandy Accelerator Mass Spectrometry facility (Kubik and Christi, 2010). All ^{10}Be/^{9}Be ratios were normalized to the ICN 01-5-1 standard with a nominal value of ^{10}Be/^{9}Be = 2.81 × 10^{-11} (Nishiizumi et al., 2007) and using a ^{10}Be half-life of 1.387 ± 0.012 m.y. (Chmeleff et al., 2010; Korschinek et al., 2010). Surface exposure ages were calculated using the CRONUS online age calculator, version 2.2 (Balco et al., 2008). Aware of ongoing debate and studies regarding geomagnetic corrections (Balco et al., 2009), we made no correction for geomagnetic field variations. The results for standards, blank, and model age calculation are given in the footnote of Tables 1 and in Table 2. The measured skyline shielding was negligible (inclination from sampling site <8°) in all directions for all sites. Therefore, ages were not corrected for topographic obstruction. Obviously, for a desert like Makran, no vegetation shielding had to be considered either. The ages presented in the Results and Discussion sections and in figures were calculated using scaling schemes from Stone (2000) modified after Lal (1991).

All ^{10}Be surface exposure ages reported in the Results section were calculated assuming no erosion or weathering and zero inheritance (Table 2). To overcome nuclide inheritance components, two depth profiles were measured and 12 modern channels with the same quartz-rich lithologies as in adjacent sampling sites were sampled. Estimated values for surface erosion are based on the surface condition of sampled terraces and depth profile measurements. The model ages corrected for inheritance and differing erosion rates are also given in Table 2.

Radiocarbon Dating of Marine Terraces

Wavecut marine terraces form well-developed, steep-like elevation with sharp (well-defined) cap-rock deposits all along coastal Makran. In contrast to fluvial terraces, they have been studied in more detail (Vita-Finzi, 1975; Page et al., 1979; Reyss et al., 1999). They cover unconformably what generally are Miocene–Pliocene marly-silty deposits. The number and the height of terraces vary from a single level 6 m above sea level at the western end of Makran, to 11 levels in Konarak (Fig. 2) where the highest terrace is 147 m above sea level (Fig. 5F).

Four shell samples (pecten and clams; Figs. 5D and 5E) were collected for ^{14}C dating from four marine terraces between Konarak and Beris (Table 3; Figs. 2 and 5). The ^{14}C was analyzed at the Laboratory of Ion Beam Physics at ETH Zurich. After graphitization, the carbon isotopic ratios were measured using accelerator mass spectrometry (Synal et al., 2007). The ^{14}C ages were calibrated using the OxCal version 4.1 open source program (http://c14.arch.ox.ac.uk/oxcalhelp/hlp_contents.html; Bronk Ramsey, 2009) and the IntCal09 calibration curve (Reimer et al., 2009). Scanning electron microscopy showed that the aragonite texture is well preserved in the dated samples (Fig. 6).

Incision and Uplift Rate

To quantify incision rates from in situ–produced cosmogenic nuclides, we sampled strath surfaces. The studied river terrace deposits are characterized by a very sharp and well-defined basal unconformity and thickness of alluvial cap (Fig. 4; Table 2). The duration of surface occupation, a period of steady discharge and sediment flux (Pazzaglia and Brandon, 2001), is difficult to determine. We assumed that the river did not spend much more time than measurement uncertainties at a particular surface, and that the measured exposure ages correspond to the abandonment time of the strath at that relative elevation. Hence, we calculated the mean rate of fluvial incision from the ratio of terrace elevation with respect to the present river level versus the abandonment TCN age of the terrace. The uncertainties on incision rates accumulate uncertainties on measured elevations and uncertainties on the timing of strath preservation from exposure ages (Table 2).

This approach is relatively reliable for the western catchments, where tectonic influence was visibly limited and where river profiles are consistent with steady state. Equating incision and uplift rates where local tectonics has clearly affected the terraces is less accurate. In that case, incision of strath terraces roughly records rock uplift, and, if there is little erosion of the bedrock, rock uplift will essentially be equivalent to surface uplift (Bishop, 2007). We therefore applied the same method for the four studied catchments to elucidate the spatial and temporal incision and/or uplift pattern over a wide area of the wedge (Fig. 7). For this study, the elevation of marine terraces has been corrected using the global sea-level curve of Lambeck and Chappell (2001) to estimate the elevation at the time of deposition (Table 3).

RESULTS

Site Description and ^{10}Be Abandonment Ages

The sampled terraces exhibited homogeneous, clast-supported profiles (Fig. 4C). The lack of remarkable lithostratigraphic identities and soil horizons prevented regional correlation. Therefore, the only criteria used with due caution was initially based on the height above the associated modern channel and, in some cases, the alluvial thickness (Table 1). These two criteria are inadequate where local tectonics has clearly affected the landscape. In such places, we had to rely on quantitative age comparisons.

The studied catchments (Fig. 3) are described from west to east. Terraces are described according to their locality, specified with an initial letter, and their elevation with respect to the present-day channel. They were numbered from top downward (for instance, O-T1 highest to O-T4 lowest at site O; Figs. 2 and 4G). They could be tracked along lengthy sections of all studied rivers, upstream from the lower ~30 km of each river, where the waterways cut through and meander on the easily eroded late Miocene marls and Pleistocene deposits of the coastal plain. We first present minimum, uncorrected ^{10}Be TCN ages. Modeled ages corrected for inheritance and erosion are given in Table 2.

Sedij Catchment

Two sites 100 km apart (A and B, Fig. 2) were investigated in the Sedij catchment. At both sites the main river is a bedrock channel. T1 and T2 strath terraces of the two sites are morphologically well correlated thanks to their near continuity for ~170 km of river distance from near Konardar in the north to near Majgi in the south (Fig. 2).

At site A (Fig. 2), terraces A-T1 and A-T2 (both <2 m thick) stand 42 m and 21 m above the present-day river, respectively (Fig. 8). Their even thickness over long distances suggests that the area was tectonically stable during the period represented by these degradational terraces, which are both underlain by sand-dominated Miocene turbitides. A-T2 is a paired surface that stretches continuously for several kilometers, whereas A-T1 is more disrupted. In addition to the A-T1 and A-T2 surfaces, we sampled a local T2 level (NA-T2) 30 km to the north of site A to further constrain the age of this regionally extensive geomorphological level.

At site B (Fig. 2), three extended flat strath surfaces (B-T1–B-T3) stand 33, 16, and 7 m above the present-day river (Fig. 8). The highest, B-T1, has been sampled for temporal correlation with terraces of site A.

Samples made of 1–2-cm-thick pieces a few centimeters across, chopped off from the surface of quartz-rich cobbles in the modern channel, were collected at sites A (A-mch) and B (B-mch) to examine nuclide inheritance.

The abandonment ages of the strath terraces sampled at sites A and B correlate very well

TABLE 2. CALCULATED EXPOSURE AGES AND INCISION RATES FOR DIFFERENT CATCHMENTS IN MAKRAN

Sample number	Local terrace name	Strath elevation (m above sea level)	Thickness (m)	River bed elevation (m)	Incision (m)	Minimum exposure age (no erosion, no inheritance) (ka)	Incision rate (mm/a)	Model exposure age* (erosion rate 0.5 mm/k.y., corrected to inheritance) (ka)	Incision rate (mm/a)	Model exposure age* (erosion rate 1 mm/k.y., corrected to inheritance) (ka)	Incision rate (mm/a)
Sedij catchment											
Q-Mak-10-36	A-T1	411	1.5	369	42 ± 2	90 ± 9	0.47	78 ± 8	0.53	80 ± 8	0.52
Q-Mak-10-37	A-T2	388	0.8	368	20 ± 1	22 ± 2	0.91	7 ± 1	2.80	7 ± 1	2.80
Q-Mak-10-38	NA-T2	471	0.7	462	9 ± 1	19 ± 1	0.47	4 ± 1	2.25	4 ± 1	2.25
Q-Mak-09-41	B-T1	241	1	201	40 ± 3	100 ± 10	0.40	80 ± 8	0.50	83 ± 9	0.48
Fanuj catchment											
Q-Mak-09-49	C-T1	417	1.5	366	51 ± 1	59 ± 5	0.85	48 ± 5	1.06	49 ± 5	1.04
Q-Mak-09-45	C-T6	373	3	369	4 ± 0.5	13 ± 1	0.31	1 ± 1	4.00	1 ± 1	4
Q-Mak-10-40	D-T1	300	1.3	256	44 ± 1	86 ± 8	0.51	76 ± 8	0.58	80 ± 8	0.55
Q-Mak-09-56	E-T1	941	2.7	921	20 ± 3	119 ± 11	0.17	117 ± 12	0.17	124 ± 13	0.16
Q-Mak-09-57	E-T2	931	3	923	8 ± 3	15 ± 1	0.53	8 ± 1	1.00	8 ± 1	1
Q-Mak-09-10	F-T2	180	0.9	151	29 ± 0.5	67 ± 9	0.43	55 ± 9	0.53	57 ± 10	0.5
Q-Mak-11-23	F-T1	130	2.5	92	38 ± 1	87 ± 8	0.44	76 ±7	0.50	78 ± 8	0.48
Q-Mak-10-44	G-T1	464	1–3	438	26 ± 4	174 ± 16	0.16	158 ± 16	0.16	169 ± 18	0.15
Q-Mak-10-45	G-T2	369	2–4	366	3 ± 0.2	55 ± 5	0.05	28 ± 3	0.11	28 ± 3	0.1
Nikshahr catchment											
Q-Mak-10-28	J-T1	240	1.5	132	108 ± 2	135 ± 12	0.80	128 ± 13	0.84	135 ± 15	0.8
Q-Mak-10-31	J-T4	144	2	99	45 ± 0.8	49 ± 4	0.90	35 ± 3	1.28	36 ± 4	1.25
Q-Mak-11-21	I-T1	281	1.7	242	39 ± 1	132 ± 12	0.29	129 ± 13	0.26	137 ± 15	0.28
Q-Mak-11-15	I-T2	302	2.1	273	29 ± 1	87 ± 8	0.33	81 ± 8	0.36	84 ± 9	0.34
Q-Mak-11-13	I-T3	220	2.3	209	11 ± 0.3	42 ± 4	0.26	33 ± 3	0.33	34 ± 3	0.32
Q-Mak-10-56	I-T4	273	3	265	8 ± 2	20 ± 2	0.40	12 ± 1	0.66	12 ± 1	0.66
Q-Mak-11-12	H-T1	759	1.8	708	51 ± 1	110 ± 11	0.46	93 ± 10	0.55	97± 11	0.52
Pishin catchment											
Q-Mak-11-01	P-T1	135	3	97	38 ± 1	99 ± 9	0.38	81 ± 8	0.47	84 ± 9	0.45
Q-Mak-11-02	P-T2	116	2.3	102	14 ± 1	34 ± 3	0.40	13 ± 2	1.07	13 ± 2	1.07
Q-Mak-09-62	O-T1	265	1	150	115 ± 2	168 ± 15	0.68	154 ± 15	0.75	166 ± 18	0.69
Q-Mak-09-32	O-T3	209	1.2	150	59 ± 0.5	95 ± 8	0.62	74 ± 7	0.80	77 ± 7	0.76
Q-Mak-10-22	O-T4	117	2	102	15 ± 0.5	26 ± 3	0.58	5 ± 2	3.00	5 ± 2	3
Q-Mak-10-19	N-T1	321	>30	254	67 ± 5	379 ± 43	0.18	399 ± 56	0.17	506 ± 99	0.13
Q-Mak-11-09	N-T2	391	4	341	50 ± 2	217 ± 21	0.23	197 ± 21	0.25	217 ± 26	0.23
Q-Mak-10-14	N-T3	283	15	260	23 ± 3	139 ± 14	0.17	106 ± 12	0.22	113 ± 13	0.2
Q-Mak-10-20	N-T4	290	9	254	36 ± 2	120 ± 11	0.30	87 ± 8	0.41	90 ± 9	0.4
Q-Mak-10-03	NN-T1	558	5	483	75 ± 2	222 ± 21	0.34	209 ± 23	0.36	231 ± 28	0.32
Q-Mak-10-23	M-T1	545	7	522	23 ± 4	138 ± 13	0.16	113 ± 12	0.20	119 ± 13	0.19
Q-Mak-10-46	K-T1	327	0.5	243	84 ± 4	47 ± 4	1.79	21 ± 2	4.00	21 ± 2	4
Q-Mak-10-47	K-T2	264	0.6	243	21 ± 3	35 ± 3	0.60	9 ± 1	2.33	9 ± 1	2.3
Q-Mak-11-18	L-T1	117	3.2	61	56 ± 2	174 ± 15	0.32	151± 26	0.37	162 ± 30	0.34
Q-Mak-11-19	L-T2	84	1.8	61	23 ± 2	125 ± 11	0.18	95 ± 9	0.24	99 ± 10	0.23
Marine terrace											
Q-Mak-12-02	M-T-12-02	77	—	—	127	73 ± 6	1.7	41 ± 4	—	42 ± 4	—

*Model exposure ages corrected for inheritance and erosion rates by subtracting ^{10}Be concentrations of depth profiles and modern channels from measured concentrations of the samples in corresponding sites. Standard atmosphere calculated using the CRONUS-Earth (Balco et al., 2008) version 2.2. A constant production rate model and scaling scheme for spallation of Lal (1991) and Stone (2000) are used. The reference spallogenic ^{10}Be production rate used of 4.49 ± 0.39 atoms/g/yr (± 1σ, SLHL [sea level, high latitude]) and monogenic production after Heisinger et al. (2002).

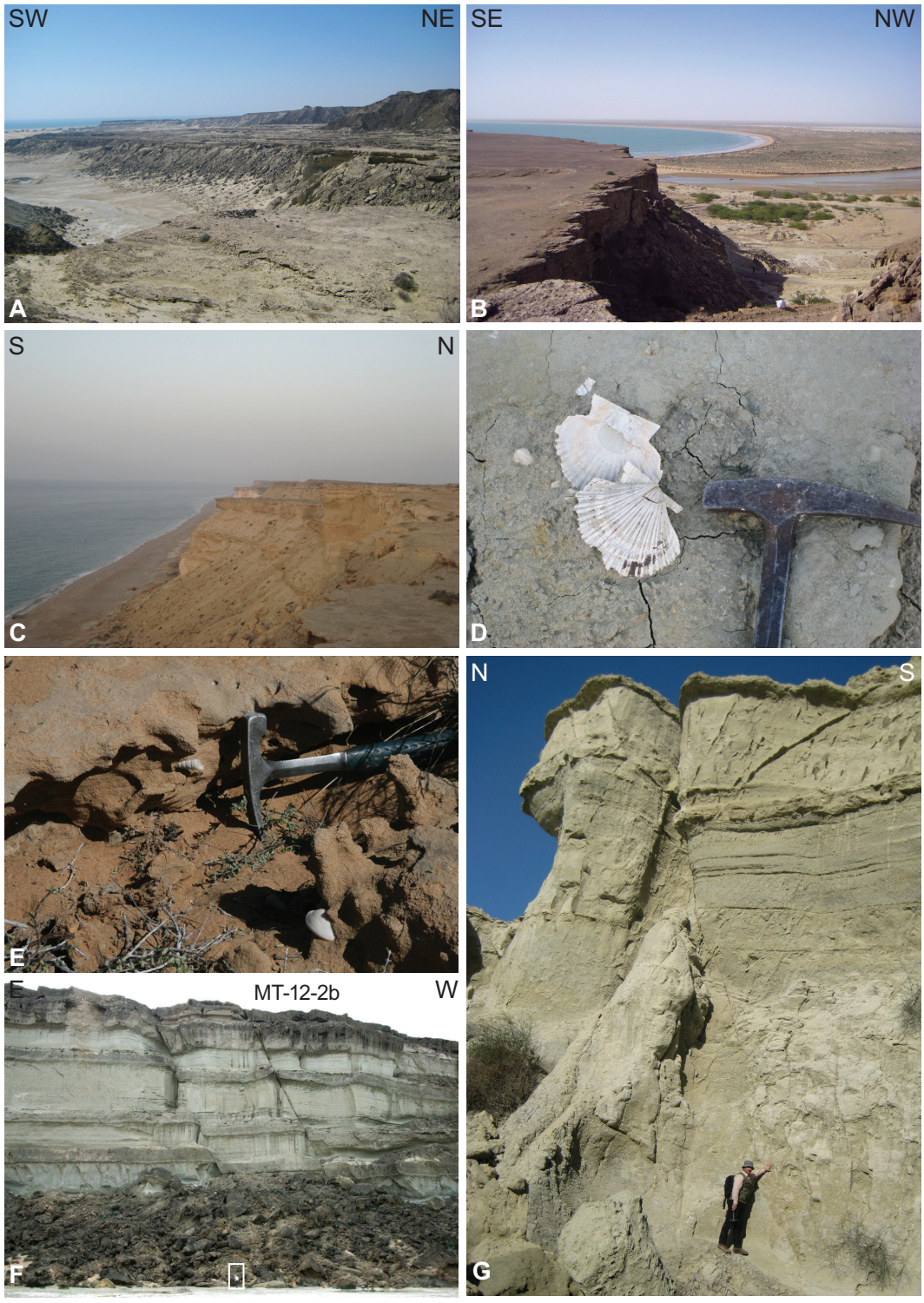

Figure 5. Photographs of marine terraces along the coast of Makran. Nearby cities are shown in Figure 2, excepted Sedij, which is just to the west of figure boundary. (A) Near Sedij (GPS: 25°32′59.18″N, 58°50′55.75″E). (B) Near Gurdim (25°21′28.57″N, 60°6′54.64″E). (C) Between Chabahar and Beris (25°14′10.20″N, 60°53′25.00″E). (D) Shells sampled for ^{14}C dating close to Sedij (25°32′51.00″N, 58°50′40.00″E). (E) Shells sampled for ^{14}C dating near Beris (25°11′44.90″N, 61°5′11.50″E). (F) Normal faults cutting marine terraces at Konarak (25°21′10.63″N, 60°18′14.10″E); white box indicates human for scale. (G) Normal fault pointed out by M. Faridi (scale) and cutting marine terraces close to Sedij (25°35′26.90″N, 58°48′29.30″E).

numerically and morphologically (Table 1 and Fig. 8), clustering at 19 ± 1 ka for T2 and 100 ± 8 ka for T1. All data in the age-elevation plot fall in the 95% interval bounds, which indicates a uniform spatial-temporal incision rate (Fig. 7). The calculated mean fluvial incision rate since abandonment is 0.35 mm/a. The exceptionally high incision rate (0.91 mm/a) obtained from the A-T2 surface reveals fast tectonic uplift at the sampling site, which pushed A-T2 10 m higher than its equivalent level (NA-T2). In most places, we tried to collect samples from the modern channel similar lithology to the one collected from the terrace surfaces.

Fanuj Catchment

We mapped the terraces of the two largest rivers (Guredak to the west and Fanuj to the east), which merge at ~35 km from the mouth of the Fanuj catchment. The two rivers display bedrock and mixed alluvial-bedrock channels along

TABLE 3. SUMMARY OF DATING ON MARINE TERRACES, INCLUDING NEW AGES FROM THIS STUDY

Location (west to east)	Sample name	Latitude (E)	Longitude (N)	Present sample elevation (m)	Sea-level position at the time of deposition (m)	Uplift (m)	Uplift rate (mm/a)	^{14}C age (yr B.P.)	Calibrated ^{14}C age (yr B.P.)	^{230}Th/^{234}U age (ka)	Reference
Jask											
	J-1	—	—	6	6	0	0	—	34,310 ± 3000	133 ± 13	Page et al., 1979
	J-2	—	—	NR		0	0	—	28,010 ± 1660		Page et al., 1979
	J-3	—	—	NR		0	0	—	32,680 ± 2550		Page et al., 1979
	J-4	—	—	NR		0	0	—	26,025 ± 1050	136 ± 14	Page et al., 1979
	HAR-1115	—	—	NR		0	0	25,610 ± 640	—		Vita-Finzi, 1975
	HAR-1907	—	—	NR		0	0	23,390 ± 400	—		Vita-Finzi, 1975
	JA13	25°38′11″	57°45′59″	>2	–1	3	0.1	>24,000	—		Reyss et al., 1999
Konarak											
	K4			5.5	–7.5	13	2.6	5520 ± 165	5935 ± 165		Page et al., 1979
	K10			2.5	–6	8.5	1.7	5190 ±120	5595 ± 120		Page et al., 1979
	K12			1.5	–6	7.5	1.5	5280 ±160	5700 ± 160		Page et al., 1979
	K8			14.5	6	8.5	0.06	_	25,675 ± 850	138 ± 12	Page et al., 1979
	MT-12-03	25°20′21.4″	60°37′45.3″	147 ± 3	–70	217	5.2	41,567 ±1068	41,486–45,571*		This study
Chabahar											
	CH44	25°19′10″	60°37′13″	4	–1	5	1.6	3670 ± 50	—		Reyss et al., 1999
	MT-12-02	25°20′21.4″	60°37′45.3″	41 ± 3	–70	111	2.3	41,482 ± 1057	45,381–41,427*		This study
Beris											
	MT-12-01A	25°13′38.03″	60°56′08.07″	8 ± 1	–6	14	2.8	5165 ± 25	4005–3947*		This study
	MT-12-01B	25°11′44.9″	61°05′11.5″	14 ± 1	–6	20	5	4837 ± 25	3663–3629*		This study
Gwater (Pakistan)											
	GW50	25°09′55″	61°30′07″	3	–110	113	4.25	>25,000			Reyss et al., 1999
Omara (Pakistan)				4	–1	5	0.1	2710 ± 135			Page et al., 1979

Note: ^{14}C ages are given with 1σ error. Calibrated (cal.) ages of this study were produced with the data set IntCal09 (Reimer et al., 2009). Estimated global sea-level elevations are based on Lambeck and Chappell (2001).
*The other probabilities are shown in Figure 13.

most of their courses. Miocene sand-dominated turbidites are the main bedrock lithology.

Sites C and D are on Guderak River. Fieldwork has revealed that this river abandoned two major levels equivalent to those mapped along Sedij River (Fig. 4D).

Six terraces are preserved at site C (Figs. 2 and 8). They likely represent local base-level falls because they were not found anywhere else in the Fanuj catchment. The highest and lowest levels are standing 72 and 2 m above the contemporary channel, respectively (Fig. 8). We sampled the highest (C-T1) and lowest (C-T6) surfaces to determine the local incision rate. The obtained numeric ages are 59 ± 5 ka for C-T2 and 13 ± 1 ka for C-T5.

At site D we sampled the two prominent, paired levels D-T1 and D-T2 (Figs. 2 and 4D). The thickness of the alluvial cap, composed of thin, clast-supported fluvial pebbles, varies from 0.8 to 3 m. The obtained age on D-T1 is 86 ± 8 ka. Consistency of morphology and age correlation with terraces T1 and T2 of Sedij River made it unnecessary to date D-T2.

Two sites (E and F), separated by a meandering channel segment too short to influence the equilibrium profile, were investigated along Fanuj River (Fig. 2). The meandering part is characterized by an extensive fill terrace, which was not sampled because it is likely related to autocyclic processes.

Two terrace levels, E-T1 and E-T2, were identified at site E (Fig. 2). E-T2 is a large, broad surface 8 m above the modern steam, whereas E-T1 consists of small remnant surfaces 12 m higher than E-T2. The alluvial parts are 2 m thick for E-T1 and 5 m thick for E-T2. The obtained ages are 119 ± 11 and 15 ± 1 ka, respectively (Table 2).

Two <2-m-thick strath terraces are prominent at site F (Fig. 8). The highest level (F-T1) was sampled for regional correlation. It yielded and age of 86 ± 8 ka.

A huge alluvial fan system is developed at site G (Figs. 2 and 9) where two major, gently tilted levels (G-T1 and G-T2) were recognized and surveyed with Differential GPS (DGPS) for precise record of the tilt (Fig. 9). Based on these measurements and field observation, we concluded that this fan system is influenced by the synclinal structure against which it abuts (Fig. 9). G-T1 and G-T2 were sampled to put age constraints on the abandonment of this fan system. The ages (174 ± 16 and 55 ± 5 ka, respectively; Table 2), morphology, and very low incision rate (0.05 mm/a) differentiate these two surfaces from regional-scale terraces.

The dated terraces of the Fanuj catchment have exposure ages scattered from 13 ± 1 ka to 119 ± 9 ka (Fig. 7). Plotting age versus incision

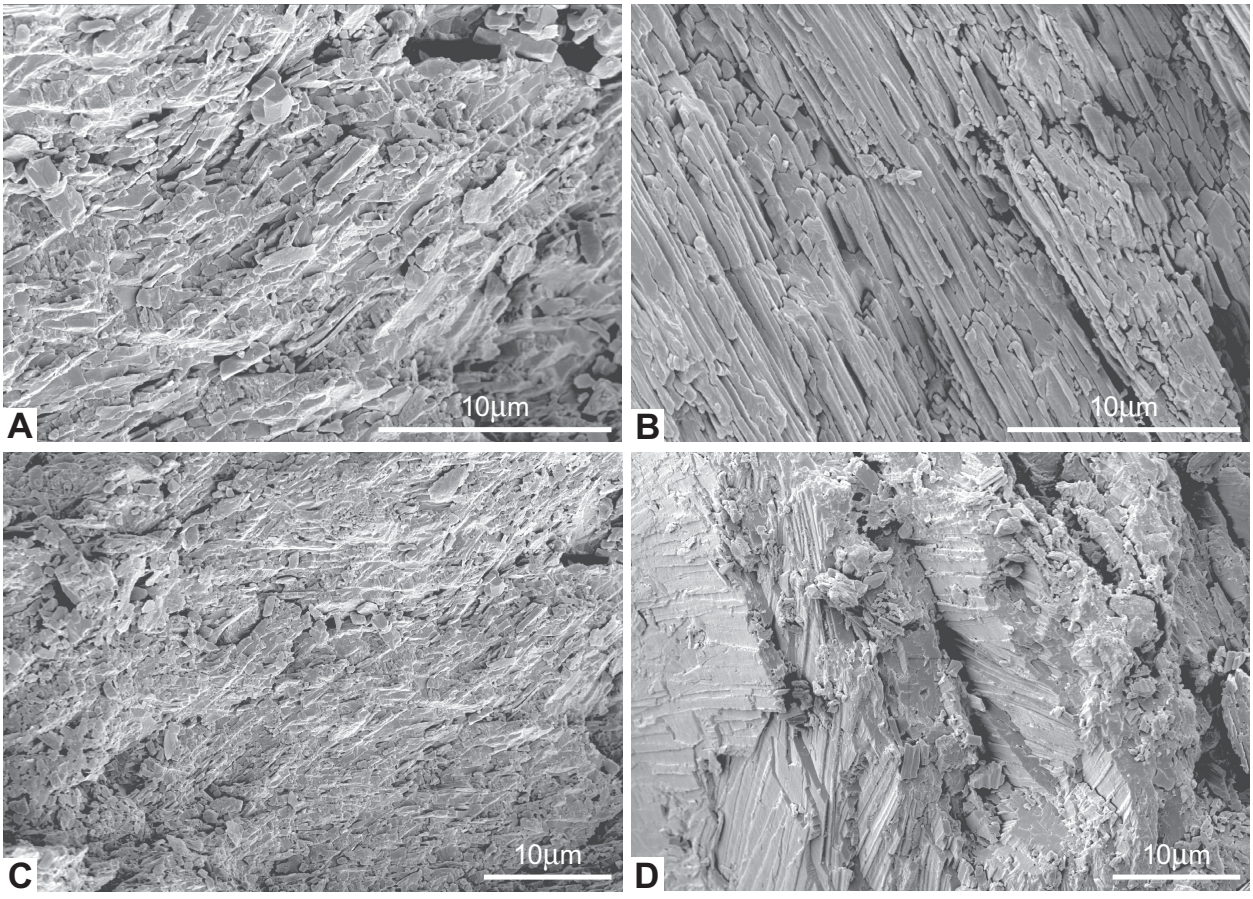

Figure 6. Scanning electron microscope images showing the well-preserved aragonite texture of dated shells. Elongate to prismatic sections and bladed crystal outlines typify primary, acicular aragonite and/or calcite pseudomorphs after aragonite.

values yields a homogeneous mean rate of 0.41 mm/a. Two samples did not fit the 95% interval confidence curve, yielding higher (C-T2) and lower (E-T1) incision rates (Fig. 7). C-T2 is one of the six staircase terraces of site C. The anomalously high incision rate (0.8 mm/a) is attributed to the recent activity of a mapped splay of the Gativan thrust (Fig. 2). Conversely, the low incision rate (0.17 mm/a) obtained from E-T1 may be inaccurate due to variations of E-T1 alluvial thickness and its fan-terrace characteristic, as exhibited by angular gravels in the trench dug into the tread. Therefore, we excluded this sample from the fluvial incision plot.

Nikshahr Catchment

Nikshahr River (Fig. 9) incised in narrow gorges in North Makran where several alluvial surfaces line the bedrock-controlled and mostly bedrock-floored channel. The matrix-supported profile of these surfaces and their thick (>20 m) colluvial cover of angular clasts (>10 cm) indicate mass-wasting and hillslope processes. Therefore we did not consider them for this work. A knickpoint at ~125 km from the mouth occurs where the river cuts through the so-called Bashakerd thrust, the tectonic boundary between North and Inner Makran (Fig. 2; Dolati, 2010). Below this location, Nikshahr River abandoned mainly <3-m-thick strath terrace deposits of fluvial gravel and pebbles on Oligocene–Miocene turbidites and marls, down to ~40 km from the coast, where the river flows onto the alluvial coastal plain.

Two levels have been mapped at site H (Fig. 2). The highest, H-T1, 51 m above the present-day channel, has been sampled for spatial and temporal correlation.

Well-preserved terraces developed large planar surfaces in tectonic basins bounded by the Ghasr-e-Ghand and Chah-Khan thrusts at sites I and J (Fig. 2). At site I, four paired levels are each capped by thin (<2 m) veneers of gravel (Fig. 10A). They are 35 (I-T1) to 16 m (I-T4) above the contemporary river bed. A sample was collected from each (Table 1). A depth profile was sampled in I-T4.

Another knickzone occurs ~80 km from the mouth, where Nikshahr River is deeply incised through the so-called Rahde-Gardz anticline (Fig. 2). Five levels of variably tilted (Fig. 10B), 1–3-m-thick strath terraces were abandoned at site J, in the downstream knickzone (Table 1). J-T1 stands 106 m and J-T5 8 m higher than the modern channel.

The ^{10}Be exposure ages of strath terraces along Nikshahr River vary between ca. 20 and 135 ka (Table 2). The mean incision rate obtained from the age-elevation plot is 0.37 mm/a (Fig. 7). J-T1 and J-T4 do not fit the 95% interval confidence boundary. This spatial change in incision rate is attributed to ongoing amplification of the Rahde-Gardz anticline (Haghipour et al., 2012).

Pishin Catchment

The Pishin catchment has a northwest-southeast orientation that makes it different from other catchments, where the main rivers flow nearly north-south. We surveyed fluvial terraces in the two main trunks, Peer Sohrab in the west and Sarbaz in the east (Fig. 2), which join together ~60 km from the mouth. Noting that the spacing between the mouths of the Sedij, Fanuj,

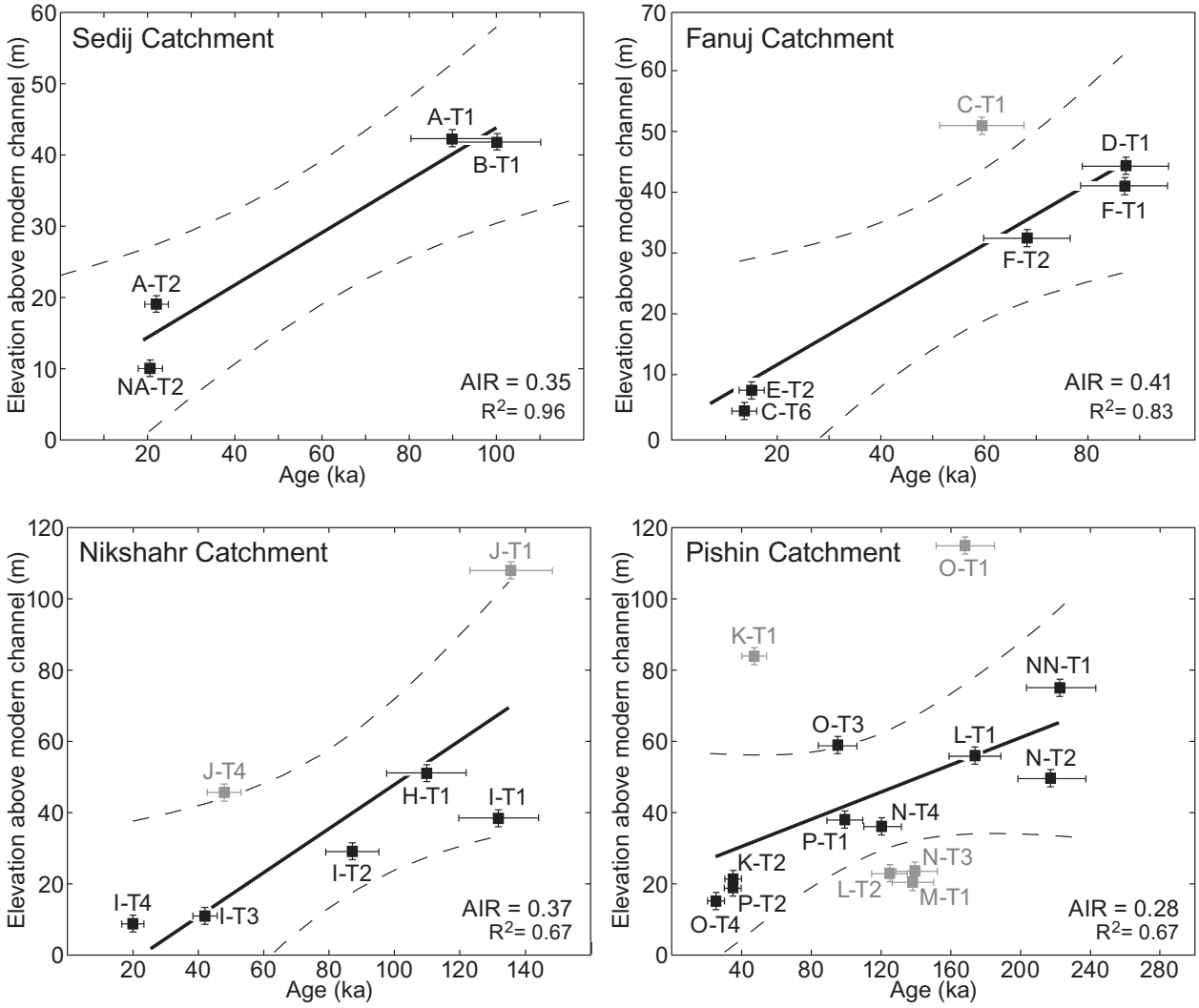

Figure 7. Incision plots for studied catchments. Solid black lines are weighted linear regression; dashed lines are envelopes showing 95% confidence limits on the age-incision relationship. AIR—apparent incision rate calculated from weighted linear regression; R^2—coefficient of determination. Sample locations are shown in Figure 8 and Table 1. Grey samples are outside the 95% confidence limits.

and Nikshahr Rivers is regular, and about half that between the Nikshahr and Pishin mouths (Fig. 3), we suspect that the Peer Sohrab River has been deviated eastward and joined the Sarbaz River. The upstream part of both rivers incised upper Eocene to lower Miocene turbidites of Inner Makran (Fig. 2). Both rivers are deflected from their bulk north-south flow direction along the northern side of the anticlinal ridge in the hanging wall of the Gativan thrust. Further south (on the middle parts of the rivers), the studied fluvial terraces were mainly located on Miocene siltstone and marl with calcareous sandstone.

Two sites were investigated along the Peer Sohrab River, which displays two prominent knickpoints, one where it cuts the Gativan thrust (~115 km from its mouth) and the other where it cuts the Chah-Khan thrust (Fig. 2). Three strath terraces were distinguished at site K, where the river cuts the Gativan thrust. We sampled the highest (K-T1, 79 m above the modern channel) and the lowest (K-T3, 15 m above the modern channel) terraces. The alluvial caps of these two levels are very thin (<1 m). The same three levels have been dated between sites K and L by Kober et al. (2013).

Site L is located ~50 km (straight distance) from site K (Fig. 2). The two extensive, paired strath terrace levels 56 m (L-T1) and 23 m (L-T2) above the present river channel were sampled. L-T1 is folded. Its alluvial part consists of ~3 m of consolidated, coarse conglomerate. L-T2 is a planar surface that extends for several kilometers.

Five sites were investigated along Sarbaz River, which is divided into four segments by the three knickpoints that coincide with the still-active Pishamak (between Northern and Inner Makran), Gativan (the most prominent), and Chah-Khan thrusts (Fig. 2; Haghipour and Burg, 2014).

Site M, on a main west-east–flowing tributary (Fig. 2), exposes three terrace levels. We sampled only M-T1, which has 7-m-thick fluvial fill and stands 23 m above the present-day river channel.

Site N (Figs. 2 and 11) also shows three terrace levels characterized by thick (>30 m), clast-supported alluvial fills representing a massive aggradational stage (Figs. 4E and 4F). This volume of alluvium was not observed anywhere

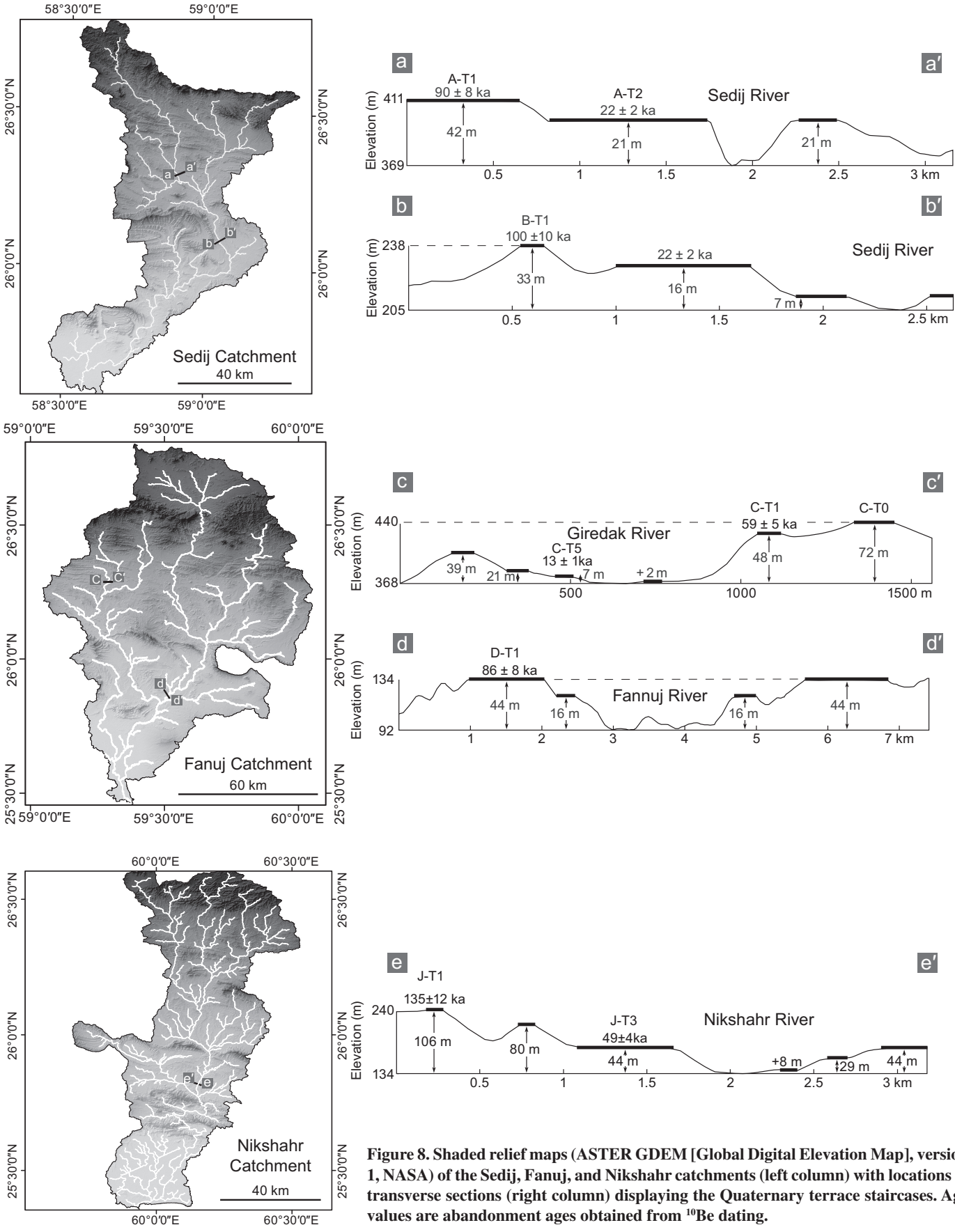

Figure 8. Shaded relief maps (ASTER GDEM [Global Digital Elevation Map], version 1, NASA) of the Sedij, Fanuj, and Nikshahr catchments (left column) with locations of transverse sections (right column) displaying the Quaternary terrace staircases. Age values are abandonment ages obtained from ^{10}Be dating.

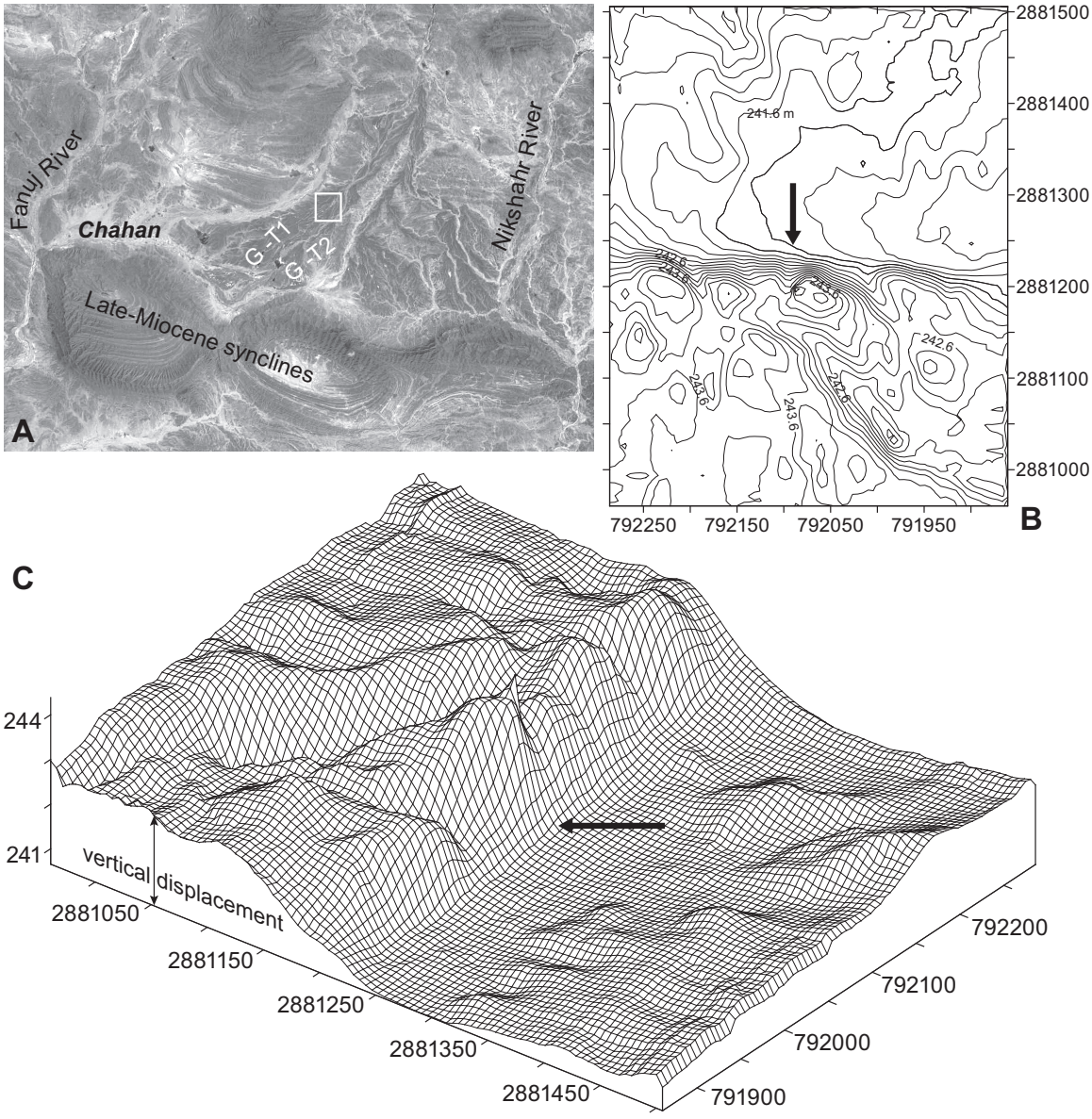

Figure 9. (A) Satellite image of the Chahan fan system blocked by late Miocene synclines (site G, Fig. 2). (B) Contour map derived from Differential Global Positioning System (DGPS) survey on terrace G-T1 (white box in A); the steep linear topographic gradient is interpreted as the scar of an active thrust fault. Contour labels are in m. (C) Three-dimensional plot of the fault scarp vertically offsetting the G-T1 surface by ~2 m. The black arrows on B and C indicate the steep gradient. UTM coordinate system used in B and C.

else. After field observation, we determined that these terraces were related to rapid filling of east-west–trending, flat synclinal basins within which the river course has been deflected behind the ramp and/or fault-propagation anticline formed on the hanging wall of the Gativan thrust (Dolati, 2010; Fig. 2). The lack of lake deposits suggests that these intra-mountainous basins were not closed, but the growth of the ramp anticline partly obstructed the river flow. We collected samples from these three paired levels, which are 67, 43, and 36 m above the modern channel. N-T1 is tilted (Fig. 4E). We took samples from a depth profile in N-T3. A very high terrace (NN-T1, 4-m-thick fluvial deposits, 75 m higher than the modern channel) was sampled near Firuzabad, to the north of site N (Fig. 2), for correlation.

At site O (Fig. 2), four strath terraces stand 113 (O-T1) to 57 m (O-T4) higher than the present-day Sarbaz River (Fig. 4G). They represent an abandoned, now-dry stream flowing into the adjacent Torbat catchment, largely developed in Pakistan. The geomorphological characteristics of site O denote capture after deposition of O-T4 of an old, topographically higher Torbat river system by the Sarbaz River (Haghipour and Burg, 2014). We collected samples from the highest (O-T1) and lowest levels (O-T4).

At site P (Figs. 2 and 11), the two paired levels P-T1 and P-T2 consist of thin (1–2 m) alluvial caps (Table 1). They can be followed for several kilometers and stand 38 and 19 m above the modern channel. Their morphology and exposure ages of 99 (P-T1) and 34 ka (P-T2) make them comparable to T1 and T2 terraces

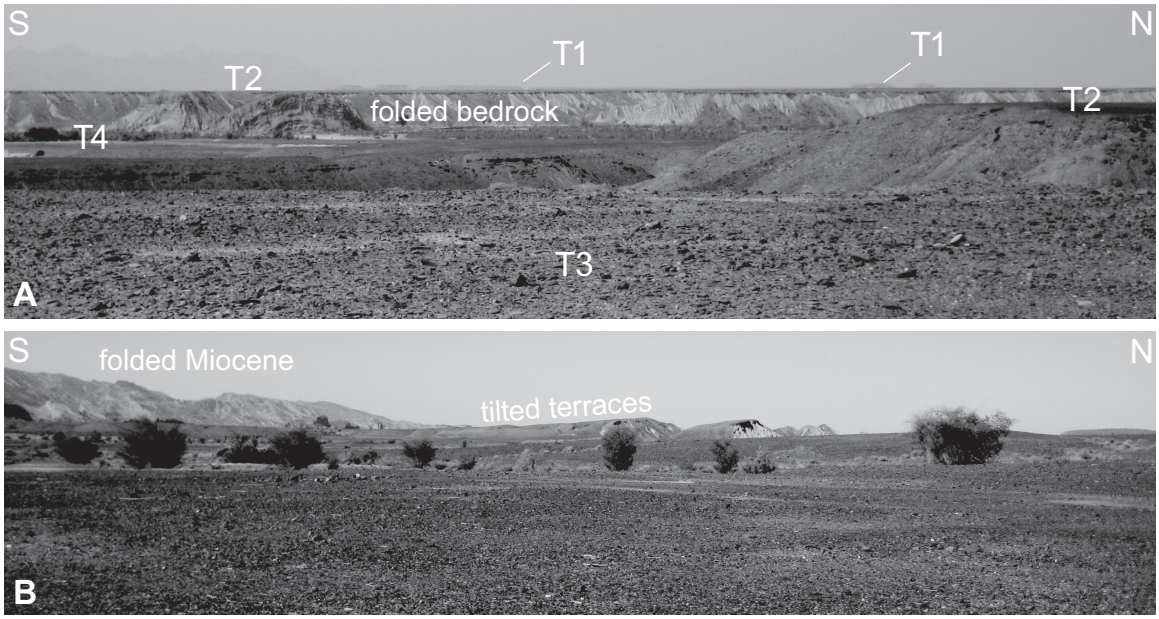

Figure 10. (A) Four levels of strath terraces at site I (Fig. 2) along Nikshahr River (GPS: 26°01′02.84″N, 60°08′41.45″E). (B) Tilted fluvial terraces at site J (Fig. 2) along Nikshahr River (25°49′19.88″N, 60°08′00.24″E).

of sites A, B, F, and H in the Sedij, Fanuj, and Nikshahr catchments. The modern channels at five sites along the Pishin catchment were sampled (Fig. 3; Table 1).

The ^{10}Be exposure ages obtained from the Pishin catchment span from ca. 20 to ca. 380 ka (Table 2). The morphological sequence of fluvial terraces differs in age from site to site along both Peer Sohrab and Sarbaz Rivers. Recent activity of the thrusts mapped in the geological basement is responsible for this bias and dislinkage of fluvial sequences. Consequently, the age-elevation plot does not show a good fit for all samples of this catchment. Yet, the mean incision rate derived from all samples of the Pishin catchment is 0.3 mm/a. Samples K-T1, O-T1, and O-T3 do not fall in the 95% interval confidence boundary and yield incision rates >0.3 mm/a (Table 2). This deviation reflects recent activity of the Gativan thrust and also the river capture where O-T1 and O-T3 samples were taken (Fig. 7). Conversely, samples L-T2, N-T3, and M-T1 yield incision rates of <0.2 mm/a. These samples represent fill terraces with relatively thick (>30 m) alluvial caps. The exposure ages for N-T3 and M-T1 are around 140 ka. The local presence of such thick sediments and their deep incision can be explained, in the absence of glacial evidence, by a change in local channel slope due to tectonic activity on the Gativan thrust, which also caused a local increase in discharge. Field checking confirmed this interpretation, as these surfaces are tilted and folded (Fig. 4E).

Depth Profiles

Deep depth profiles slightly more than 2 m deep were dug and sampled in terraces I-T4 (Nikshahr catchment; Fig. 12B) and N-T3 (Pishin catchment; Fig. 12A). The thickness of the alluvial cap in the two depth profiles (~2 m) is the minimum pit depth required to access the amount of TCN inheritance (Anderson et al., 1996).

We applied the geologically constrained Monte Carlo approach from the best model fit of 100,000 solutions (Hidy et al., 2010) to determine the ^{10}Be model ages of these surfaces, which are 120 ± 10 ka for N-T3 and 15 ± 1 ka for I-T4. In N-T3, the ^{10}Be concentrations plot on an almost perfect curve of exponential decrease with depth. The deepest sample in I-T4 does not fit the theoretically exponential depth versus nuclide concentration relationship (e.g., Anderson et al., 1996; Gosse and Phillips, 2001). Excluding this sample from the simulation, the other measurements fit well the downward exponential decrease in ^{10}Be nuclide concentration. This agreement falls in line with the principle of longevity of desert pavement stability (e.g., Haff and Werner, 1996; Matmon et al., 2009). No stratigraphic feature or internal bedding was found in these two depth profiles. Their homogeneity (Fig. 12) strongly suggests that sedimentation of the gravel happened during one event over a short time period. Accordingly, we assumed a constant bulk density (~2.4 g/cm^3) of sediment through the terrace profiles. The estimated inheritance from best fit in N-T3 is 1.1 × 10^5 atoms/g SiO_2 and 0.4 × 10^5 atoms/g SiO_2 in I-T4. This result indicates that inheritance may alter ages younger than 20 ka but has a very small effect on the dating of older terraces.

Active Channels

Another approach to estimate the inherited nuclide component is to analyze samples from the active channel (Repka et al., 1997; Hancock et al., 1999), assuming that erosion and discharge have not changed since the deposition time. However, the assumption behind this approach is not systematic and may lead to misinterpretation of true ages (e.g., Schaller et al., 2004). We collected 11 amalgamated samples from the active main trunks to determine present-day cosmogenic inheritance (Table 1).

The ^{10}Be concentration in modern channel samples varies between 0.5 × 10^5 and 2.1 × 10^5 atoms/g. These values are equivalent to apparent ages of 11 ± 1 ka and 48 ± 4 ka, respectively. The agreement between concentration accumulated in river bed samples and concentration from depth profile samples (Table 1) suggests that the current source of pebbles has not significantly changed over the last few thousand years. The similarity of concentration in modern channels and the lowest terrace surfaces (e.g., C-mch and C-T6, K-mch and K-T2, Table 1) further suggests that modern samples are reworked from older terraces. Yet, the ^{10}Be concentrations in the

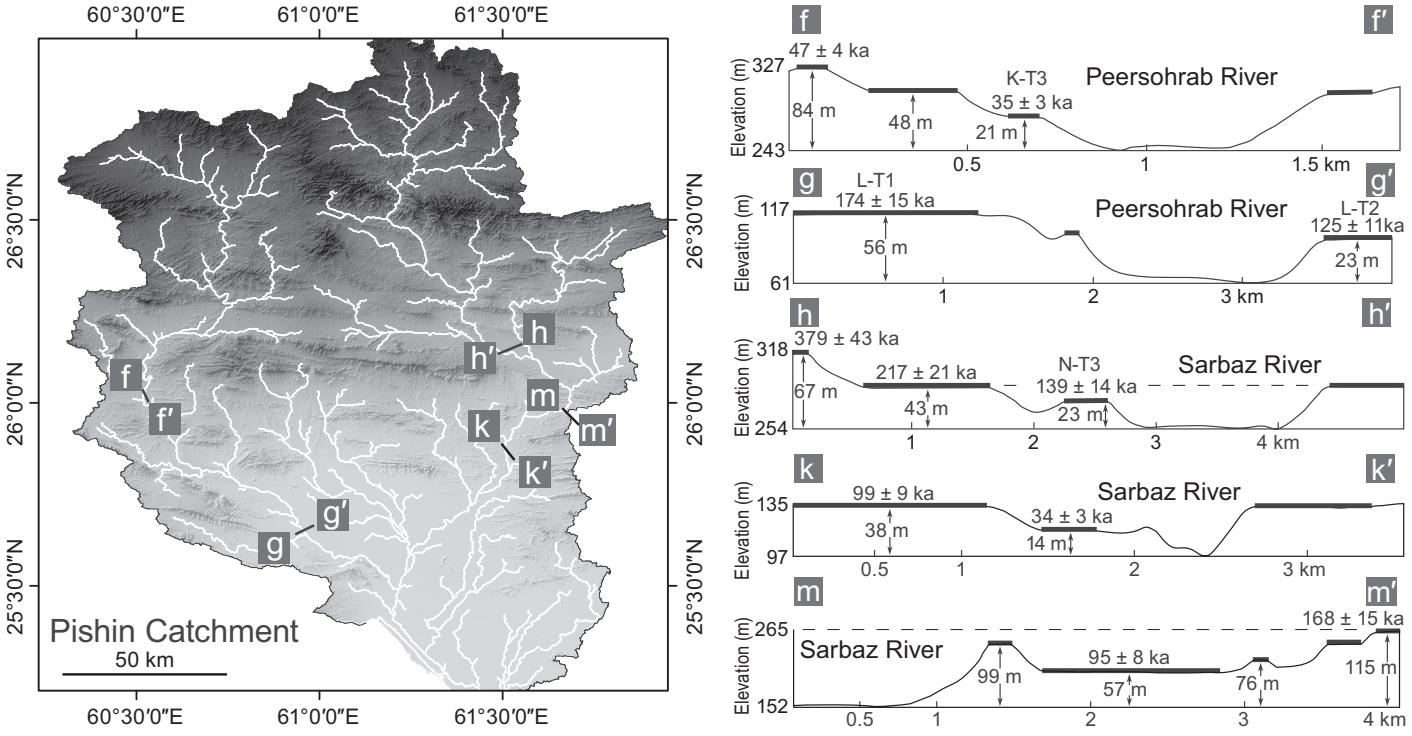

Figure 11. Shaded relief map (ASTER GDEM [Global Digital Elevation Map], version 1, NASA) of the Pishin catchment (left) with trace of transverse sections (right) displaying the Quaternary terrace staircases. Age values are abandonment ages obtained from ^{10}Be dating.

two depth profiles are lower than those of modern channels. Therefore, concentration values from modern channels cannot be used as the amount of the inheritance component everywhere.

^{14}C Dating of Marine Terraces

The ^{14}C ages obtained from our samples cluster in two groups: Holocene (MT-12-01A at 5165 ± 25 yr B.P. and MT-12-01B at 4873 ± 25 yr B.P.) and Pleistocene (MT-12-02 at 41,482 ± 1057 yr B.P. and MT-12-03 at 41,567 ± 1068 yr B.P.; Table 3; Fig. 13). Calculated uplift rates are 1.7–2.3 mm/a for Pleistocene terraces and 2.5–5 mm/a for Holocene terraces. These rates are higher than previously reported but still indicate an increase in Holocene time as pointed out by Page et al. (1979). However, our new Pleistocene ages are very close to the limit of ^{14}C dating; therefore, they must be considered as minimum ages, and caution should be taken for interpretation.

Comparison Between Incision Rate and River Gradient

In general, the average K_{Sn} values increase eastward with a positive relationship between channel steepness and incision rate (Fig. 14). The K_{Sn} values and calculated incision rates do not show remarkable changes along Sedij and Fanuj Rivers. Conversely, marked but localized changes in K_{Sn} and incision rates along Nikshahr, Sarbaz, and Peer Sohrab Rivers are clearly associated with faults and/or folds mapped in the bedrock, the Gativan thrust being the most prominent, with the highest K_{Sn} values and an incision rate of >0.5 mm/a. Therefore the spatial changes in K_{Sn} and incision rates reflect differential and tectonically driven rock uplift. Folded and tilted terraces in the vicinity of active structures are additional evidence for current deformation.

DISCUSSION

Age Uncertainties and Resolution

Although the surface exposure age method provides useful constraints on intermediate time scales (10^3–10^5 yr), the age accuracy suffers from several sources of uncertainty. In particular, TCN ages from surface clasts may be overestimated if the clasts have acquired measurable TCN concentrations prior to final deposition (inheritance). Conversely, TCN ages may be underestimated if the clasts have been recently exhumed or weathered. Inheritance uncertainties have far more impact on determining the TCN ages than uncertainties in absolute production rates and scaling factors (e.g., Ivy-Ochs et al., 2012). Total analytical errors on ages including production rates (10%), accelerator mass spectrometry measurements (3%–4%), and chemical processing (1%–2%) are ~10%–15%. The largest analytical uncertainty comes from site estimation of production rate (e.g., Gosse and Phillips, 2001). To approach uncertainties related to inheritance and erosion components, we corrected our ages to measured inheritance and erosion. Samples older than 20 ka are not affected by inheritance. Another argument for small inheritance is that we did not observe any relationship between amount of nuclide concentration and river length (longer traveling time causes more inheritance and therefore older ages). The good consistency between obtained ages and the morphostratigraphy of the terraces is further evidence for minor inheritance effect.

The surface condition and pavement of sampled terraces record very little erosion out of small, lowest-order, narrow and dry, ephemeral rills and thalwegs, and bear no anthropogenic disturbance (Figs. 4A and 4B). The preservation of terraces as old as ca. 379 ka suggests that the erosion rate is ≤1 cm/k.y. This is much smaller than the few centimeters per thousand years reported by other studies of quartz-rich river sediments in tectonically quiescent landscapes under similar climate regimes (e.g.,

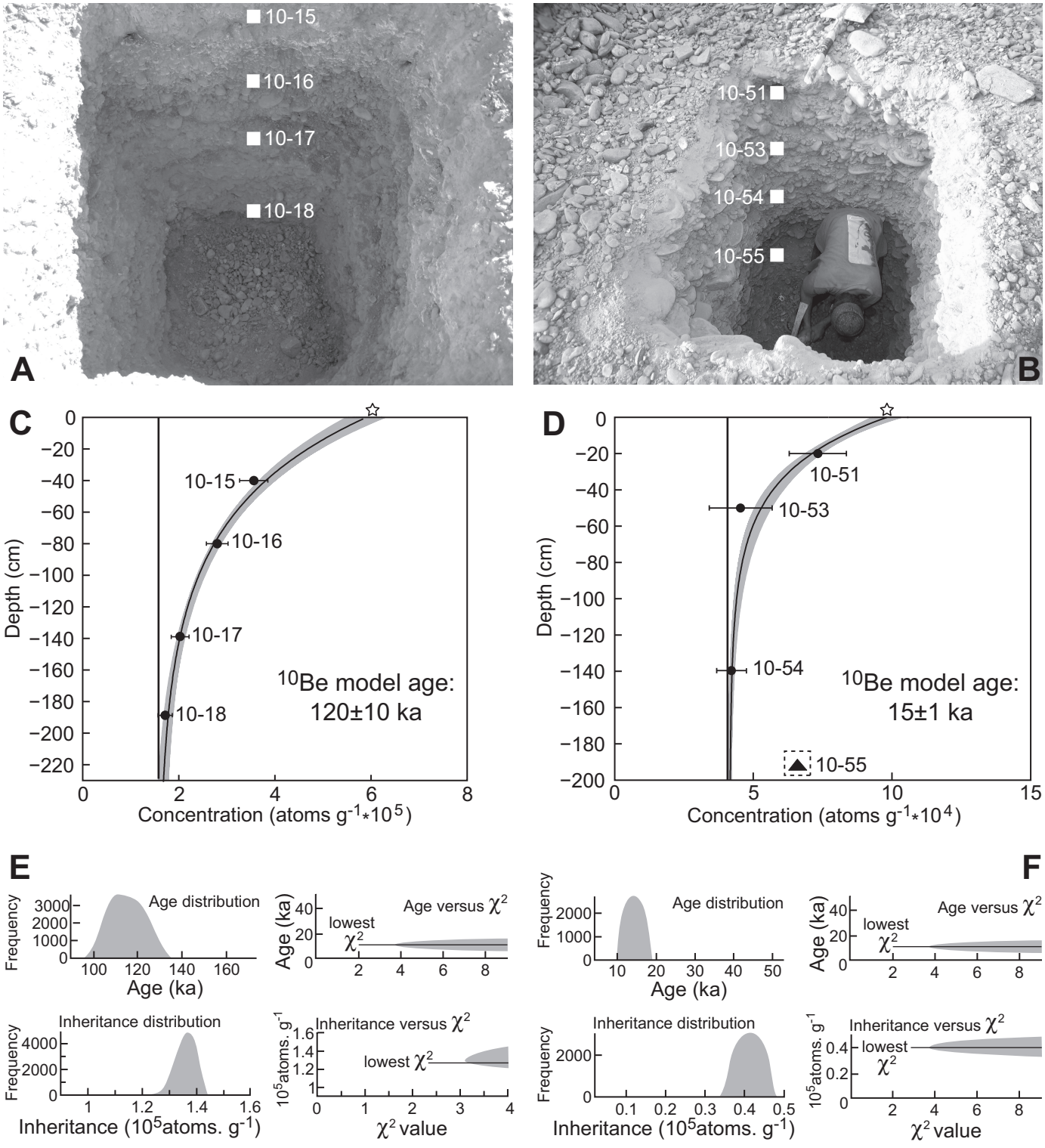

Figure 12. (A, B) Excavated pit in terrace N-T3 (A; Fig. 3; GPS: 26°08′06.04″N, 61°33′14.50″E) and pit in I-T4 (B; Fig. 3; 26°01′58.55″N, 60°08′12.16″E). Both terraces are homogeneous and clast supported without unconformity and soil. (C, D) Concentration versus depth plots with best-fit regression (curved black lines) from 100,000 Monte Carlo simulations through the samples (black circles) positioned in A and B. Grey curves cover the solution space. Stars represent the calculated concentrations in amalgamated surface samples. The bottom sample in the I-T4 profile (black triangle in D) was excluded from simulations because its nuclide concentration does not follow the theoretical depth rule. Analytical results are in Table 1. (E) Results for the 2σ age, inheritance, solution spaces for samples from the N-T3 terrace. (F) Results for the 3σ age, inheritance, solution spaces for samples from I-T4. The chi-square cutoff values are determined from the chi-square probability distribution function introduced in Hidy et al. (2010).

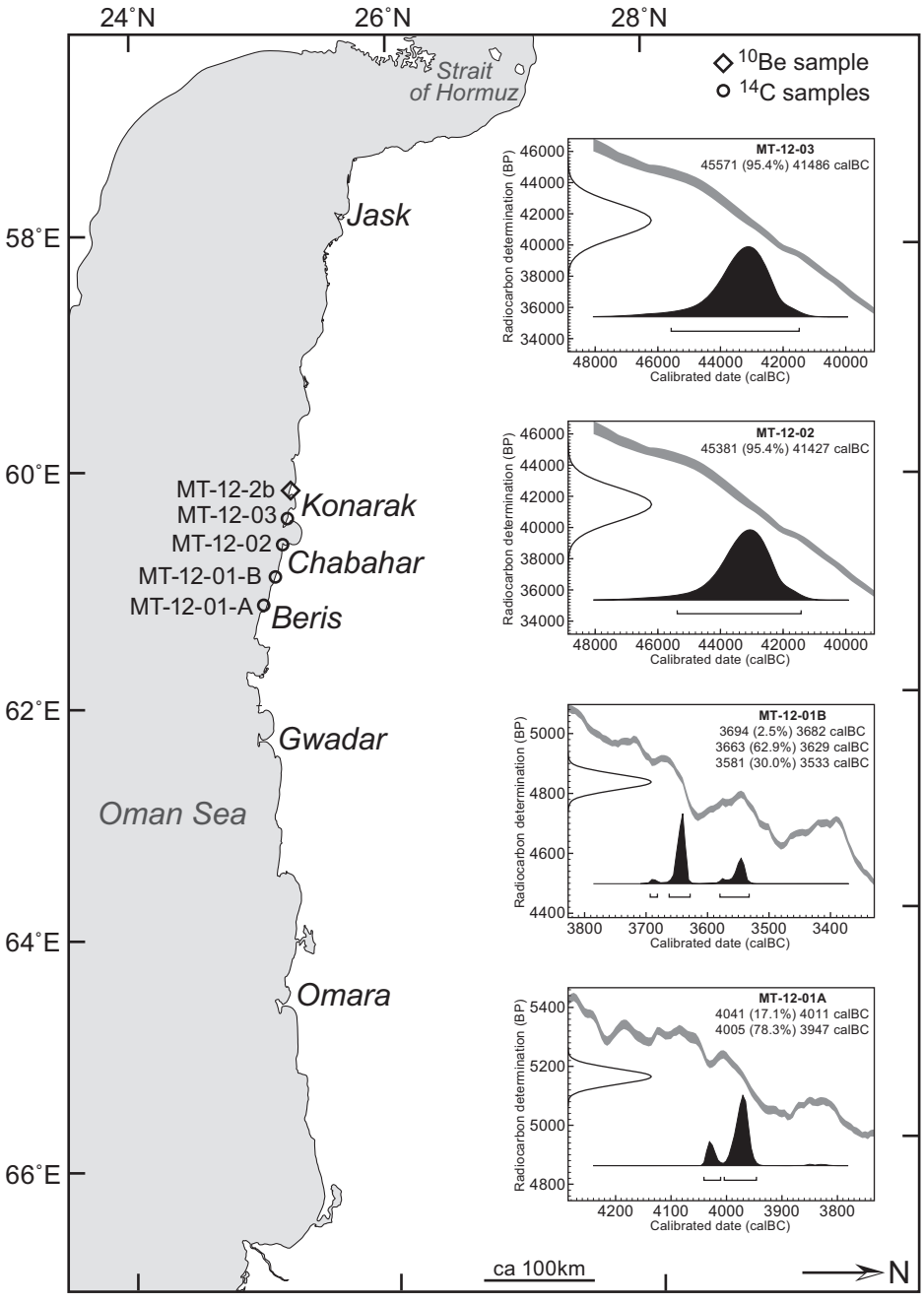

Figure 13. Location of marine terrace samples dated with ^{14}C and ^{10}Be. Inset plots represent the calculated and calibrated ^{14}C ages using the OxCal version 4.1 program (http://c14.arch.ox.ac.uk/oxcalhelp/hlp_contents.html; Bronk Ramsey, 2009). Note that the map is rotated (north to the right). The gray calibration curve shows the relationship between true ^{14}C age (on the *y*-axis) and true calendar age on the *x*-axis, The white curve on the *y*-axis shows ^{14}C determination derived by measurement. The black curve shows the age probability. calBC—calendar B.C.

Clapp et al., 2002; Matmon et al., 2009). The estimated erosion rate from the space solution plot for the old N-T3 surface is 0.07 cm/k.y., and 0.05 cm/k.y. for the younger I-T4 surface. These results, based on minimum age values, confirm that the mean erosion rate is very low. Because there is no independent estimate of erosion rate in Makran and adjacent areas, we modeled the exposure ages for a constant maximum denudation rate of 1 cm/a while allowing for net erosion to vary between 0 and 30 cm using the approach of Hidy et al. (2010) (Table 2).

Age Correction and Resolution

One may dispute the reliability and resolution of exposure ages, and thus the interpretation we make from their distribution, if both inheritance and erosion corrections are not introduced.

For age correction, we applied to each dated site the consistent inheritance obtained from depth profiles and modern channels (Table 2). We also applied a minimum (0.05 cm/k.y.) and maximum (1 cm/k.y.) erosion rate to generate modeled ages.

Ages between 20 and 270 ka exhibit very small (within error) shifts from uncorrected to modeled values. Accordingly, these ages have a good resolution. Conversely, ages younger than 20 and older than 270 ka shift dramatically with correction and therefore lose their robustness (Fig. 15; Table 2). Therefore the usefulness of quantitative estimates on incision rates is bracketed between these two ages.

Climatic and Tectonic Forcing

The coexistence of several levels of fluvial terraces generally results from alternating incision and aggradation events linked to rhythmic variations in climate and/or base level. An important question was whether the river dynamics were sensitive to climate variability or influenced by the tectonic evolution of the Makran wedge. The distribution of exposure ages obtained in this work helps to answer that, in Makran, both tectonic and climatic forces controlled river incision, with obvious intervention of tectonic forcing in the eastern part of the study area.

The reliable ^{10}Be exposure ages (with zero erosion and negligible inheritance) range between 20 and 270 ka. They correspond to both glacial and interglacial episodes and are interpreted as follows. (1) Age clusters between 15 and 22 ka and between 85 and 120 ka correspond to the Last Glacial Maximum MIS 2 and interglacial marine MIS 5, respectively (Fig. 15). The ~20 ka terrace has also been identified in western Makran (Regard et al., 2006). Having argued that basement erodibility is not a factor, we can only attribute the widespread consistency in age and morphological classification of the terraces belonging to these two clusters, over four adjacent catchments and away from coastal regions, to external, regional processes like climate. Moreover, stages MIS 2 and MIS 5 coincide with global formation of terraces (e.g., Bridgland and Westaway, 2008). In addition, paleoclimate studies reveal MIS 5 as a wet period in the area (e.g., Burns et al., 1998). The corresponding wide surfaces indicate that their straths were preserved during river widening. (2) Ages between 130 and 180 ka correspond to

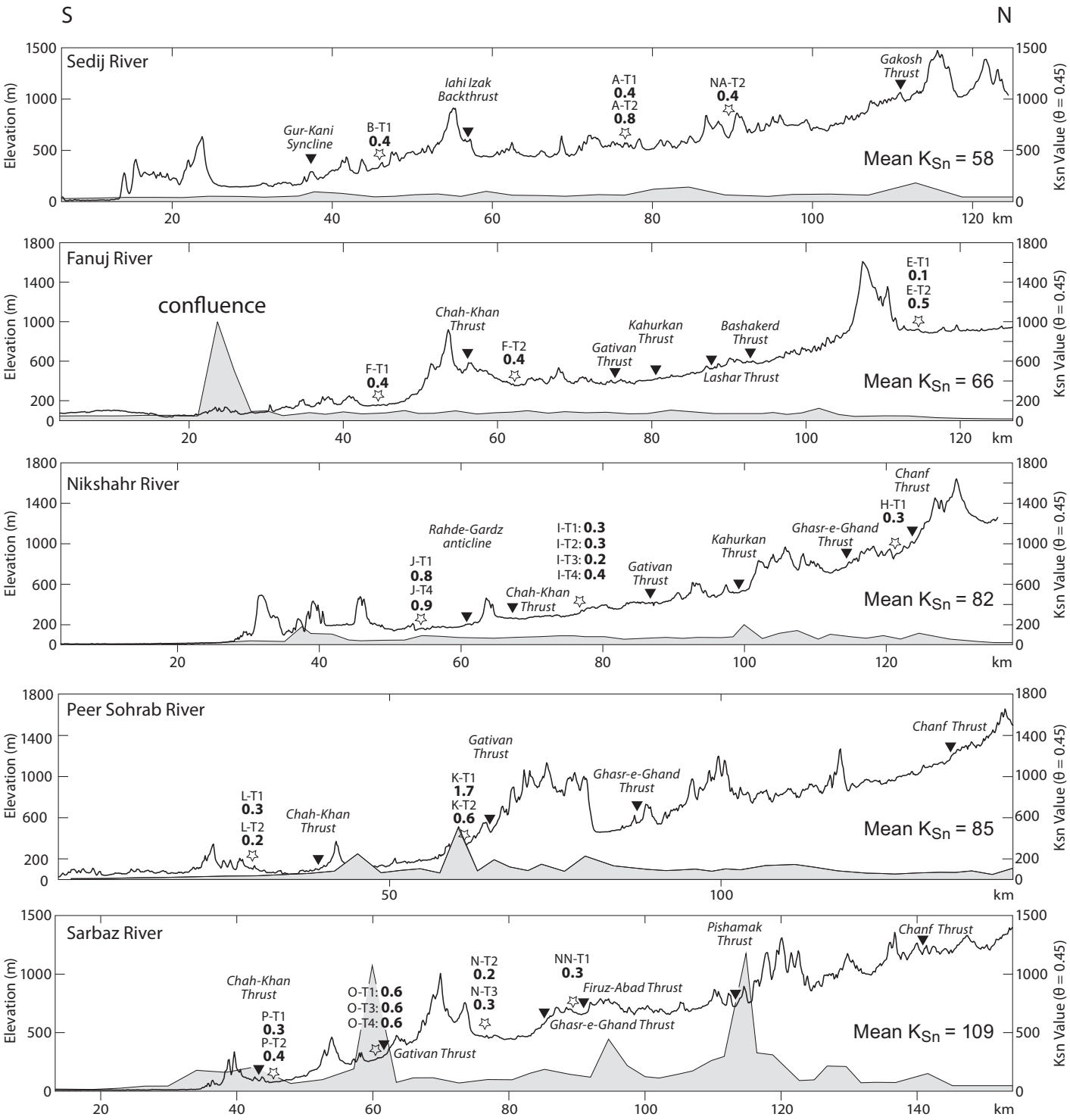

Figure 14. Normalized stream gradient (K_{Sn}) plots (shaded area) along with topography along studied rivers. θ—concavity. Bold numbers give incision rates (mm/a) determined from dated fluvial terraces (Table 2).

the glacial MIS 6. Their location on the hanging wall of active structures such as the Gativan and Chah-Khan thrusts (Haghipour et al., 2012) indicates that they represent local base-level changes in response to tectonic forces. (3) Abandonment ages between 50 and 60 ka correspond to MIS 3 (Fig. 15). They were obtained from local and narrow surfaces in the Fanuj catchment (Fig. 8). Field evidence suggests that they are the products of lateral incision subsequent to transient disturbance of the main river channel. (4) The terraces dated at 220 ka (i.e., MIS 7) are wide and continuous. The incision rates derived from these surfaces (~0.3 mm/a) match the regional steady-state rate and also the 180–

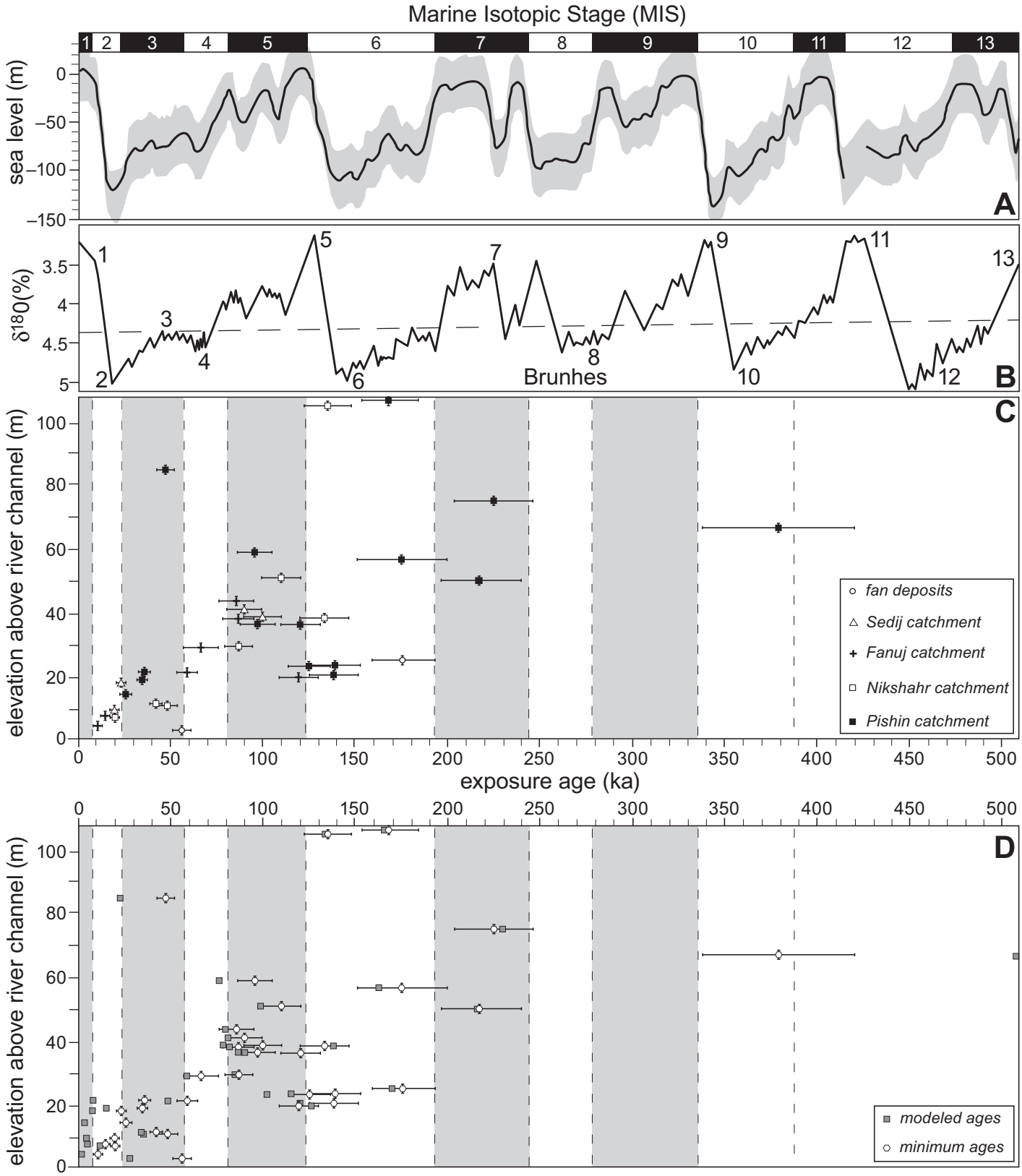

Figure 15. Terrace correlation based on ^{10}Be surface exposure dating plotted with the eustatic curve for the last 500 k.y. (A) Marine isotopic stages (MIS) corresponding to glacial (even numbers) and interglacial (odd numbers) periods; numbers in top bar. (B) Deep-sea δ^{18}O stable isotopes, after Chappell et al. (1996). (C) Uncorrected ^{10}Be ages represented with their error bars (1σ). (D) Corrected ^{10}Be ages using inheritance of each site (Table 2) and a maximum erosion rate of 0.7 cm/k.y. (Table 2).

200 ka continental pluvial period recorded in the speleothems of Hoti cave in northern Oman (Fleitmann et al., 2003). These two observations suggest climate-driven formation. The >5-m-thick alluvial deposits indicate aggradation. (5) Terraces younger than 20 ka and older than 270 ka are difficult to interpret because surface erosion and nuclide inheritance may have disturbed the actual age.

In summary, the widespread consistency of dated surfaces and the inferred steady-state incision rate (~0.3–0.5 mm/a) support that climate fluctuations played a role in terrace development. The globally most accepted reason for climate-driven genesis of terraces is glacial-interglacial transition (Westaway, 2002). However, the standard error in TCN numeric ages does not allow such precision in this study. The measured age populations corresponding to MIS 2, 5, and 7 in Makran have a 100 k.y. periodicity comparable to that of the Milankovitch cycles over the last 500 k.y. (Hays et al., 1976), which supports the interpretation of the corresponding terrace abandonment as climatic signals. In contrast, the scattered preservation of terraces yielding unsteady incision rates (>0.5 mm/a) near active faults and folds indicates tectonic forcing on the formation of disconnected surfaces. This conclusion is further supported by coincidence of high incision rates with high K_{Sn} values and field observation of structures with typical geomorphological traits of active tectonics. However, equally strong monsoons in the northern Arabian Sea in both glacial and interglacial stages have been reported (Clemens and Prell, 2003).

Uplift Rates

Incision can be used as a proxy for tectonic uplift if incision kept pace with regional uplift (e.g., Burbank and Anderson, 2001; Pazzaglia and Brandon, 2001) and the river were not adjusting to isostatic and/or eustatic changes. Some studies argued that a river never reaches a state of equilibrium, so that its terraces cannot be used to infer vertical tectonic movement (Kiden and Tornqvist, 1998). We did not observe any sign of reoccupation of the straths by a younger channel, and we excluded fill terraces for incision and/or uplift rate calculation. The results show that the mean rates of fluvial incision in Pleistocene times (regionally ~0.3 mm/a) are similar to uplift rates previously inferred from marine terraces of the Iranian Makran coast (0.1–0.4 mm/a; Page et al., 1979). This similarity suggests that the same tectonic regime caused uplift of both the fluvial terraces and the marine terraces together. This is likely the surface uplift rate subsequent to distributed internal strain in the onshore Makran accretionary wedge. Coastal uplift was apparently faster in Holocene times (2 mm/a after Page et al. [1979], 3 mm/a in this study). The difference in Pleistocene and Holocene uplift rates does not appear in uncorrected data of the studied fluvial terraces. Therefore, we attribute high Holocene coastal uplift rates to surface uplift along the shoulders of large normal faults (Figs. 5F and 5G) known near the coast and offshore (Grando and McClay, 2007; Burg et al., 2012). However, direct comparison of geologic process rates in different time scales is not always reliable because these processes depend on the measured time interval (Gardner et al., 1987).

CONCLUSION

We produced absolute ages of the fluvial terraces over a large area of the onshore Makran accretionary wedge. The ^{10}Be exposure ages range between 13 and 380 ka. Terraces younger than 20 ka and older than 270 ka are difficult to interpret because surface erosion and nuclide inheritance may have disturbed the actual ages. These results highlight the problems one may face in dating surfaces assuming no erosion and negligible inheritance for very old (>300 ka) or very young (<20 ka) terraces in regions like Makran, with semi-arid climate and moderate tectonic activity.

Rivers have drained and erodeed central Makran since at least 340 ka and have, since then, undergone several cycles of incision and aggradation.

Two major, regional levels are correlatable over the four adjacent catchments mapped in central Makran. This geographically widespread correspondence suggests that the genesis of these two terrace levels is associated with a regional, climatically driven force at the transition between glacial and interglacial periods. The older probably dates from MIS 5; the younger correlates with MIS 2.

The comparison of incision rates in different, adjacent catchments enables distinguishing between a regional mean rate of 0.3–0.4 mm/a and higher (0.8–1 mm/a) local incision and/or uplift rates. The similarity between regional fluvial incision rates and Pleistocene coastal uplift rates (0.2 mm/a) constrained by uplifted marine terraces supports the inference that rivers in the study area responded to a long-term interplay between climatically driven incision and tectonically driven surface uplift in this region. The latter reflects uniform, steady-state wedge growth during Quaternary times. However, perfect steady state is unlikely on short length scales, with local instabilities in response to localized deformation.

ACKNOWLEDGMENTS

This work was supported by ETH project no. 0-20481-08 and the Swiss National Fund project no. 2-77644-09. Administrative and logistical support by the Geological Survey of Iran is sincerely acknowledged. We thank M. Faridi for help in the field; we acknowledge fruitful discussions with F. Kober and D. Bernoulli, who also helped for scanning electron microscopy of our shell samples. Two thorough and very constructive anonymous reviews and comments from Editor C. Koerberl and editorial board member J.J. Clark greatly improved the present manuscript.

REFERENCES CITED

Anderson, R.S., Repka, J.L., and Dick, G.S., 1996, Explicit treatment of inheritance in dating depositional surfaces using in situ ^{10}Be and ^{26}Al. Geology, v. 24, p. 47–51, doi:10.1130/0091-7613(1996)024<0047:ETOIID>2.3.CO;2.

Balco, G., Stone, J.O., Lifton, N.A., and Dunai, T.J., 2008, A complete and easily accessible means of calculating surface exposure ages or erosion rates from ^{10}Be and ^{26}Al measurements. Quaternary Geochronology, v. 3, p. 174–195, doi:10.1016/j.quageo.2007.12.001.

Balco, G., Briner, J., Finkel, R.C., Rayburn, J.A., Ridge, J.C., and Schaefer, J.M., 2009, Regional beryllium-10 production rate calibration for late-glacial northeastern North America. Quaternary Geochronology, v. 4, p. 93–107, doi:10.1016/j.quageo.2008.09.001.

Bevis, M., Taylor, F.W., Schutz, B.E., Recy, J., Isacks, B.L., Helu, S., Singh, R., Kendrick, E., Stowell, J., Taylor, B., and Calmant, S., 1995, Geodetic observations of very rapid convergence and back-arc extension at the Tonga Arc. Nature, v. 374, p. 249–251, doi:10.1038/374249a0.

Bierman, P., and Nichols, K.K., 2004, Rock to sediment—slope to sea with ^{10}Be—rates of landscape change. Annual Review of Earth and Planetary Sciences, v. 32, p. 215–255, doi:10.1146/annurev.earth.32.101802.120539.

Bilotti, F., and Shaw, J.H., 2005, Deep-water Niger Delta fold and thrust belt modeled as a critical-taper wedge: The influence of elevated basal fluid pressure on structural styles. American Association of Petroleum Geologists Bulletin, v. 89, p. 1475–1491, doi:10.1306/06130505002.

Bishop, P., 2007, Long-term landscape evolution: Linking tectonics and surface processes. Earth Surface Processes and Landforms, v. 32, p. 329–365, doi:10.1002/esp.1493.

Blum, M.D., and Törnqvist, T.E., 2000, Fluvial responses to climate and sea-level change: A review and look forward. Sedimentology, v. 47, p. 2–48, doi:10.1046/j.1365-3091.2000.00008.x.

Blum, M.D., Misner, T.J., Collins, E.S., Scott, D.B., Morton, R.A., and Aslan, A., 2001, Middle Holocene sea-level rise and highstand at +2 m, central Texas coast. Journal of Sedimentary Research, v. 71, p. 581–588, doi:10.1306/112100710581.

Brandon, M.T., Roden-Tice, M.K., and Garver, J.I., 1998, Late Cenozoic exhumation of the Cascadia accretionary wedge in the Olympic Mountains, northwest Washington State. Geological Society of America Bulletin, v. 110, p. 985–1009, doi:10.1130/0016-7606(1998)110<0985:LCEOTC>2.3.CO;2.

Bridgland, D., and Westaway, R., 2008, Climatically controlled river terrace staircases: A worldwide Quaternary phenomenon. Geomorphology, v. 98, p. 285–315, doi:10.1016/j.geomorph.2006.12.032.

Bronk Ramsey, C., 2009, Bayesian analysis of radiocarbon dates. Radiocarbon, v. 51, p. 337–360.

Bull, W.B., 2009, Tectonically Active Landscapes: Chichester, Wiley-Blackwell, 326 p.

Burbank, D.W., and Anderson, R.S., 2001, Tectonic Geomorphology. Malden, Oxford, Blackwell Science, 273 p.

Burbank, D.W., Beck, R.A., and Mulder, T.J., 1994, The Himalayan foreland basin, *in* Yin, A., and Harrison, T.M., eds., Tectonic Evolution of Asia. Cambridge, UK, Cambridge University Press, p. 149–188.

Burg, J.-P., Bernoulli, D., Smit, J., Dolati, A., and Bahroudi, A., 2008, A giant catastrophic mud-and-debris flow in the Miocene Makran. Terra Nova, v. 20, p. 188–193, doi:10.1111/j.1365-3121.2008.00804.x.

Burg, J.-P., Dolati, A., Bernoulli, D., and Smit, J., 2012, Structural style of the Makran Tertiary accretionary complex in SE-Iran, *in* Al Hosani, K., Roure, F., Ellison, R., and Lokier, S., eds., Lithosphere Dynamics and Sedimentary Basins: The Arabian Plate and Analogues. Heidelberg, Springer Verlag, p. 239–259.

Burns, S.J., Matter, A., Frank, N., and Mangini, A., 1998, Speleothem-based paleoclimate record from northern Oman. Geology, v. 26, p. 499–502, doi:10.1130/0091-7613(1998)026<0499:SBPRFN>2.3.CO;2.

Byrne, D.E., Sykes, L.R., and Davis, D.M., 1992, Great thrust earthquakes and aseismic slip along the plate boundary of the Makran Subduction Zone. Journal of Geophysical Research, v. 97, p. 449–478, doi:10.1029/91JB02165.

Caley, T., Malaizé, B., Zaragosi, S., Rossignol, L., Bourget, J., Eynaud, F., Martinez, P., Giraudeau, J., Charlier, K., and Ellouz-Zimmermann, N., 2011, New Arabian Sea records help decipher orbital timing of Indo-Asian monsoon. Earth and Planetary Science Letters, v. 308, p. 433–444, doi:10.1016/j.epsl.2011.06.019.

Chappell, J., Omura, A., Esat, T., McCulloch, M., Pandolfi, J., Ota, Y., and Pillans, B., 1996, Reconciliaion of late Quaternary sea levels derived from coral terraces at Huon Peninsula with deep sea oxygen isotope records. Earth and Planetary Science Letters, v. 141, p. 227–236, doi:10.1016/0012-821X(96)00062-3.

Chmeleff, J., von Blanckenburg, F., Kossert, K., and Jakob, D., 2010, Determination of the ^{10}Be half-life by multicollector ICP-MS and liquid scintillation counting. Nuclear Instruments & Methods in Physics Research: Section B, Beam Interactions with Materials and Atoms, v. 268, p. 192–199.

Clapp, E.M., Bierman, P.R., and Caffee, M., 2002, Using ^{10}Be and ^{26}Al to determine sediment generation rates and identify sediment source areas in an arid region drainage basin. Geomorphology, v. 45, p. 89–104, doi:10.1016/S0169-555X(01)00191-X.

Clemens, S.C., and Prell, W.L., 2003, A 350,000 year summer-monsoon multi-proxy stack from the Owen Ridge, Northern Arabian Sea. Marine Geology, v. 201, p. 35–51, doi:10.1016/S0025-3227(03)00207-X.

Dahlen, F.A., 1990, Critical taper model of fold-and-thrust belts and accretionary wedges. Annual Review of Earth and Planetary Sciences, v. 18, p. 55–99, doi:10.1146/annurev.ea.18.050190.000415.

Davis, D., Suppe, J., and Dahlen, F.A., 1983, Mechanics of fold-and-thrust belts and accretionary wedges. Journal of Geophysical Research, v. 88, p. 1153–1172, doi:10.1029/JB088iB02p01153.

DeCelles, P.G., and Mitra, G., 1995, History of the Sevier orogenic wedge in terms of critical taper models, northeast Utah and southwest Wyoming. Geological Society of America Bulletin, v. 107, p. 454–462, doi:10.1130/0016-7606(1995)107<0454:HOTSOW>2.3.CO;2.

Degens, E.T., and Paluska, A., 1979, Tectonic and climatic pulses recorded in Quaternary sediments of the Caspian–Black Sea region. Sedimentary Geology, v. 23, p. 149–163, doi:10.1016/0037-0738(79)90012-5.

Djamali, M., de Beaulieu, J.-L., Shah-hosseini, M., Andrieu-Ponel, V., Ponel, P., Amini, A., Akhani, H., Leroy, S.A.G., Stevens, L., Lahijani, H., and Brewer, S., 2008, A late Pleistocene long pollen record from Lake Urmia, NW Iran. Quaternary Research, v. 69, p. 413–420, doi:10.1016/j.yqres.2008.03.004.

Dolati, A., 2010, Stratigraphy, structural geology and low-temperature thermochronology across the Makran accretionary wedge in Iran [Ph.D. thesis]. Zurich, ETH Zurich, 309 p.

Falcon, N.L., 1975, From Musandam to the Iranian Makran. The Geographical Journal, v. 141, p. 55–58, doi:10.2307/1796945.

Farhoudi, G., and Karig, D.E., 1977, Makran of Iran and Pakistan as an active arc system. Geology, v. 5, p. 664–668, doi:10.1130/0091-7613(1977)5<664:MOIAPA>2.0.CO;2.

Fleitmann, D., Burns, S.J., Neff, U., Mangini, A., and Matter, A., 2003, Changing moisture sources over the last 330,000 years in northern Oman from fluid-inclusion evidence in speleothems. Quaternary Research, v. 60, p. 223–232, doi:10.1016/S0033-5894(03)00086-3.

Flint, J.J., 1974, Stream gradient as a function of order, magnitude and discharge. Water Resources Research, v. 10, p. 969–973, doi:10.1029/WR010i005p00969.

Frankel, K.L., Brantley, K.S., Dolan, J.F., Finkel, R.C., Klinger, R.E., Knott, J.R., Machette, M.N., Owen, L.A., Phillips, F.M., Slate, J.L., and Wernicke, B.P., 2007, Cosmogenic ^{10}Be and ^{36}Cl geochronology of offset alluvial fans along the northern Death Valley fault zone: Implications for transient strain in the eastern California shear zone. Journal of Geophysical Research, v. 112, B06407, doi:10.1029/2006JB004350.

Friend, P.F., Jones, N.E., and Vincent, S.J., 2009, Drainage evolution in active mountain belts: Extrapolation backwards from present-day Himalayan river patterns, Fluvial Sedimentology VI. Blackwell Publishing Ltd., v. 28, p. 305–313.

Gahalaut, V.K., and Catherine, J.K., 2006, Rupture characteristics of 28 March 2005 Sumatra earthquake from GPS measurements and its implication for tsunami generation. Earth and Planetary Science Letters, v. 249, p. 39–46, doi:10.1016/j.epsl.2006.07.015.

Gardner, T.W., Jorgensen, D.W., Schuman, C., and Lemieux, C.R., 1987, Geomorphic and tectonic process rates: Effect of measured time interval. Geology, v. 15, p. 259–261, doi:10.1130/0091-7613(1987)15<259:GATPRE>2.0.CO;2.

Gosse, J.C., and Phillips, F.M., 2001, Terrestrial in situ cosmogenic nuclides: Theory and application. Quaternary Science Reviews, v. 20, p. 1475–1560, doi:10.1016/S0277-3791(00)00171-2.

Grando, G., and McClay, K., 2007, Morphotectonics domains and structural styles in the Makran accretionary prism, offshore Iran. Sedimentary Geology, v. 196, p. 157–179, doi:10.1016/j.sedgeo.2006.05.030.

Hack, J.T., 1957, Studies of longitudinal stream profiles in Virginia and Maryland. U.S. Geological Survey Professional Paper 294-B, p. 45–97.

Haff, P.K., and Werner, B.T., 1996, Dynamical processes on desert pavements and the healing of surficial disturbances. Quaternary Research, v. 45, p. 38–46, doi:10.1006/qres.1996.0004.

Haghipour, N., and Burg, J.-P., 2014, Geomorphological analysis of the drainage system on the growing Makran accretionary wedge. Geomorphology, v. 209, p. 111–132, doi:10.1016/j.geomorph.2013.11.030.

Haghipour, N., Burg, J.-P., Kober, F., Zeilinger, G., Ivy-Ochs, S., Kubik, P.W., and Mohammadi, F., 2012, Rate of crustal shortening and non-Coulomb behaviour of an active accretionary wedge: The folded fluvial terraces in Makran (SE, Iran). Earth and Planetary Science Letters, v. 355–356, p. 187–198, doi:10.1016/j.epsl.2012.09.001.

Hancock, G.S., Anderson, R.S., and Whipple, K.X., 1998, Beyond power: Bedrock river incision process and form, *in* Tinkler, K., and Wohl, E. E., eds., Rivers over Rock: Fluvial Processes in Bedrock Channels. American Geophysical Union Geophysical Monograph 107, p. 35–60.

Hancock, G.S., Anderson, R.S., Chadwick, O.A., and Finkel, R.C., 1999, Dating fluvial terraces with ^{10}Be and ^{26}Al profiles: Application to the Wind River, Wyoming. Geomorphology, v. 27, p. 41–60, doi:10.1016/S0169-555X(98)00089-0.

Hartshorn, K., Hovius, N., Dade, W.B., and Slingerland, R.L., 2002, Climate-driven bedrock incision in an active mountain belt. Science, v. 297, p. 2036–2038, doi:10.1126/science.1075078.

Hays, J.D., Imbrie, J., and Shackleton, N.J., 1976, Variations in the Earth's orbit: Pacemaker of the ice ages. Science, v. 194, p. 1121–1132, doi:10.1126/science.194.4270.1121.

Heisinger, B., Lal, D., Jull, A.J.T., Kubik, P., Ivy-Ochs, S., Knie, K., and Nolte, E., 2002, Production of selected cosmogenic radionuclides by muons: 2. Capture of negative muons. Earth and Planetary Science Letters, v. 200, p. 357–369, doi:10.1016/S0012-821X(02)00641-6.

Hidy, A.J., Gosse, J.C., Pederson, J.L., Mattern, J.P., and Finkel, R.C., 2010, A geologically constrained Monte Carlo approach to modeling exposure ages from profiles of cosmogenic nuclides: An example from Lees Ferry, Arizona. Geochemistry Geophysics Geosystems, v. 11, Q0AA10.

Hilley, G.E., and Arrowsmith, J.R., 2008, Geomorphic response to uplift along the Dragon's Back pressure ridge, Carrizo Plain, California. Geology, v. 36, p. 367–370, doi:10.1130/G24517A.1.

Ivy-Ochs, S., Dühnforth, M., Densmore, A.L., and Alfimov, V., 2012, Dating fan deposits with cosmogenic nuclides, *in* Schneuwly-Bollschweiler, M., ed., Dating Torrential Processes on Fans and Cones: Methods and Their Application for Hazard and Risk Assessment: Advances in Global Change Research, Volume 47. Dordrecht, Springer, p. 243–263.

Jackson, J., and McKenzie, D., 1984, Active tectonics of the Alpine-Himalayan Belt between western Turkey and Pakistan. Geophysical Journal of the Royal Astronomical Society, v. 77, p. 185–264, doi:10.1111/j.1365-246X.1984.tb01931.x.

Kehl, M., 2009, Quaternary climate change in Iran: The state of knowledge. Erdkunde, v. 63, p. 1–17, doi:10.3112/erdkunde.2009.01.01.

Kiden, P., and Tornqvist, T.E., 1998, Can river terrace flights be used to quantify Quaternary tectonic uplift rates? Journal of Quaternary Science, v. 13, p. 573–575, doi:10.1002/(SICI)1099-1417(1998110)13:6<573::AID-JQS407>3.0.CO;2-M.

Kirby, E., and Whipple, K., 2001, Quantifying differential rock-uplift rates via stream profile analysis. Geology, v. 29, p. 415–418, doi:10.1130/0091-7613(2001)029<0415:QDRURV>2.0.CO;2.

Kober, F., Zeilinger, G., Ivy-Ochs, S., Dolati, A., Smit, J., and Kubik, P.W., 2013, Climatic and tectonic control on fluvial and alluvial fan sequence formation in the Central Makran Range, SE-Iran. Global and Planetary Change, v. 111, p. 133–149, doi:10.1016/j.gloplacha.2013.09.003.

Kohl, C.P., and Nishiizumi, K., 1992, Chemical isolation of quartz for measurement of in-situ-produced cosmogenic nuclides. Geochimica et Cosmochimica Acta, v. 56, p. 3583–3587, doi:10.1016/0016-7037(92)90401-4.

Korschinek, G., Bergmaier, A., Faestermann, T., Gerstmann, U.C., Knie, K., Rugel, G., Wallner, A., Dillmann, I., Dollinger, G., von Gostomski, C.L., Kossert, K., Maiti, M., Poutivtsev, M., and Remmert, A., 2010, A new value for the half-life of ^{10}Be by Heavy-Ion Elastic Recoil Detection and liquid scintillation counting. Nuclear Instruments & Methods in Physics Research: Section B, Beam Interactions with Materials and Atoms, v. 268, p. 187–191.

Kubik, P.W., and Christl, M., 2010, ^{10}Be and ^{26}Al measurements at the Zurich 6 MV Tandem AMS facility. Nuclear Instruments & Methods in Physics Research: Section B, Beam Interactions with Materials and Atoms, v. 268, p. 880–883.

Kuhle, M., 2008, The Pleistocene glaciation (LGP and pre-LGP, pre-LGM) of SE Iranian mountains exemplified by the Kuh-i-Jupar, Kuh-i-Lalezar and Kuh-i-Hezar massifs. Polarforschung, v. 77, p. 71–88.

Lal, D., 1991, Cosmic ray labeling of erosion surfaces: In situ nuclide production rates and erosion models. Earth and Planetary Science Letters, v. 104, p. 424–439, doi:10.1016/0012-821X(91)90220-C.

Lambeck, K., and Chappell, J., 2001, Sea level change through the last glacial cycle. Science, v. 292, p. 679–686, doi:10.1126/science.1059549.

Lavé, J., and Avouac, J.-P., 2001, Fluvial incision and tectonic uplift across the Himalayas of central Nepal. Journal of Geophysical Research, v. 106, p. 26,561–26,591, doi:10.1029/2001JB000359.

Masson, F., Chéry, J., Hatzfeld, D., Martinod, J., Vernant, P., Tavakoli, F., and Ghafory-Ashtiani, M., 2005, Seismic versus aseismic deformation in Iran inferred from earthquakes and geodetic data. Geophysical Journal International, v. 160, p. 217–226, doi:10.1111/j.1365-246X.2004.02465.x.

Matmon, A., Simhai, O., Amit, R., Haviv, I., Porat, N., McDonald, E., Benedetti, L., and Finkel, R., 2009, Desert pavement–coated surfaces in extreme deserts present the longest-lived landforms on Earth. Geological

Society of America Bulletin, v. 121, p. 688–697, doi: 10.1130/B26422.1.

McCall, G.J.H., 1997, The geotectonic history of the Makran and adjacent areas of southern Iran. Journal of Asian Earth Sciences, v. 15, p. 517–531, doi:10.1016 /S0743-9547(97)00032-9.

McCall, G.J.H., 2002, A summary of the geology of the Iranian Makran, *in* Clift, P.D., Kroon, F.D., Gaedecke, C., and Craig, J., eds., The Tectonic and Climatic Evolution of the Arabian Sea Region. Geological Society of London Special Publication 195, p. 147–204.

McCall, G.J.H., and Kidd, R.G.W., 1982, The Makran, southeastern Iran: The anatomy of a convergent plate margin active from Cretaceous to present, *in* Leggett, J.K., ed., Trench-Forearc Geology: Sedimentation and Tectonics of Modern and Ancient Active Plate Margins. Geological Society of London Special Publication 10, p. 387–397.

Merritts, D., and Vincent, K.R., 1989, Geomorphic response of coastal streams to low, intermediate, and high rates of uplift, Mendocino triple junction region, northern California. Geological Society of America Bulletin, v. 101, p. 1373–1388, doi:10.1130/0016-7606 (1989)101<1373:GROCST>2.3.CO;2.

Molnar, P., Brown, E.T., Burchfiel, B.C., Qidong, D., Xianyue, F., Jun, L., Raisbeck, G.M., Jianbang, S., Zhangming, W., Yiou, F., and Huichuan, Y., 1994, Quaternary climate change and the formation of river terraces across growing anticlines on the north flank of the Tien-Shan, China. The Journal of Geology, v. 102, p. 583–602, doi:10.1086/629700.

Montgomery, D.R., and Brandon, M.T., 2002, Topographic controls on erosion rates in tectonically active mountain ranges. Earth and Planetary Science Letters, v. 201, p. 481–489, doi:10.1016/S0012-821X(02)00725-2.

Nishiizumi, K., Imamura, M., Caffee, M.W., Southon, J.R., Finkel, R.C., and McAninch, J., 2007, Absolute calibration of ^{10}Be AMS standards. Nuclear Instruments & Methods in Physics Research: Section B, Beam Interactions with Materials and Atoms, v. 258, p. 403–413.

Ochs, M., and Ivy-Ochs, S., 1997, The chemical behavior of Be, Al, Fe, Ca and Mg during AMS target preparation from terrestrial silicates modeled with chemical speciation calculations. Nuclear Instruments & Methods in Physics Research: Section B, Beam Interactions with Materials and Atoms, v. 123, p. 235–240.

Owen, L.A., Frankel, K.L., Knott, J.R., Reynhout, S., Finkel, R.C., Dolan, J.F., and Lee, J., 2011, Beryllium-10 terrestrial cosmogenic nuclide surface exposure dating of Quaternary landforms in Death Valley. Geomorphology, v. 125, p. 541–557, doi:10.1016/j.geomorph.2010 .10.024.

Page, W.D., Alt, J.N., Cluff, L.S., and Plafker, G., 1979, Evidence for the recurrence of large-magnitude earthquakes along the Makran coast of Iran and Pakistan. Tectonophysics, v. 52, p. 533–547, doi:10.1016/0040 -1951(79)90269-5.

Pazzaglia, F.J., 2013, fluvial terraces, *in* Treatise of Geomorphology, Fluvial Landforms: Elsevier, v. 9, p. 379–412.

Pazzaglia, F.J., and Brandon, M.T., 2001, A fluvial record of long-term steady-state uplift and erosion across the Cascadia forearc high, western Washington State. American Journal of Science, v. 301, p. 385–431, doi: 10.2475/ajs.301.4-5.385.

Regard, V., Bellier, O., Braucher, R., Gasse, F., Bourlès, D., Mercier, J., Thomas, J.C., Abbassi, M.R., Shabanian, E., and Soleymani, S., 2006, ^{10}Be dating of alluvial deposits from southeastern Iran (the Hormoz Strait area). Palaeogeography, Palaeoclimatology, Palaeoecology, v. 242, p. 36–53, doi:10.1016/j.palaeo.2006.05.012.

Reimer, P.J., Baillie, M.G.L., Bard, E., Bayliss, A., Beck, J.W., Blackwell, P.G., Bronk Ramsey, C., Buck, C.E., Burr, G.S., Edwards, R.L., Friedrich, M., Grootes, P.M., Guilderson, T.P., Hajdas, I., Heaton, T.J., Hogg, A.G., Hughen, K.A., Kaiser, K.F., Kromer, B., McCormac, F.G., Manning, S.W., Reimer, R.W., Richards, D.A., Southon, J.R., Talamo, S., Turney, C.S.M., van der Plicht, J., and Weyhenmeyer, C.E., 2009, IntCal09 and Marine 09 radiocarbon age calibration curves, 0–50,000 years cal BP. Radiocarbon, v. 51, p. 1111–1150.

Repka, J.L., Anderson, R.S., and Finkel, R.C., 1997, Cosmogenic dating of fluvial terraces, Fremont River, Utah. Earth and Planetary Science Letters, v. 152, p. 59–73, doi:10.1016/S0012-821X(97)00149-0.

Reyss, J.L., Pirazzoli, P.A., Haghipour, A., Hatté, C., and Fontugne, M., 1999, Quaternary marine terraces and tectonic uplift rates on the south coast of Iran, *in* Stewart, I.S., and Vita-Finzi, C., eds., Coastal Tectonics. Geological Society of London Special Publication 146, p. 225–237.

Schaller, M., von Blanckenburg, F., Hovius, N., Veldkamp, A., van den Berg, M.W., and Kubik, P.W., 2004, Paleoerosion rates from cosmogenic ^{10}Be in a 1.3 Ma terrace sequence: Response of the River Meuse to changes in climate and rock uplift. The Journal of Geology, v. 112, p. 127–144, doi:10.1086/381654.

Schmidt, S., Hetzel, R., Kuhlmann, J., Mingorance, F., and Ramos, V.A., 2011, A note of caution on the use of boulders for exposure dating of depositional surfaces. Earth and Planetary Science Letters, v. 302, p. 60–70, doi:10.1016/j.epsl.2010.11.039.

Seeber, L., and Gornitz, V., 1983, River profiles along the Himalayan arc as indicators of active tectonics. Tectonophysics, v. 92, p. 335–367, doi:10.1016/0040 -1951(83)90201-9.

Simpson, G.D.H., 2010, Formation of accretionary prisms influenced by sediment subduction and supplied by sediments from adjacent continents. Geology, v. 38, p. 131–134, doi:10.1130/G30461.1.

Sklar, L.S., and Dietrich, W.E., 1998, River longitudinal profiles and bedrock incision models: Stream power and the influence of sediment supply, *in* Tinkler, K., and Wohl, E.E., eds., Rivers over Rock: Fluvial Processes in Bedrock Channels. American Geophysical Union Geophysical Monograph 107, p. 237–260.

Smit, J., Burg, J.-P., Dolati, A., and Sokoutis, D., 2010, Effects of mass waste events on thrust wedges: Analogue experiments and application to the Makran accretionary wedge. Tectonics, v. 29, TC3003, doi:10 .1029/2009TC002526.

Smith, T.R., Merchant, G.E., and Birnir, B., 2000, Transient attractors: Towards a theory of the graded stream for alluvial and bedrock channels. Computers & Geosciences, v. 26, p. 541–580, doi:10.1016/S0098-3004 (99)00128-4.

Snead, R.J., 1992, Uplifted marine terraces along the Makran coast of Pakistan and Iran, *in* Shroder, J.F., ed., Himalaya to the Sea: Geology, Geomorphology, and the Quaternary. London, Routledge, p. 327–361.

Snyder, N.P., Whipple, K.X., Tucker, G.E., and Merritts, D.J., 2000, Landscape response to tectonic forcing: Digital elevation model analysis of stream profiles in the Mendocino triple junction region, northern California. Geological Society of America Bulletin, v. 112, p. 1250–1263, doi:10.1130/0016-7606(2000)112 <1250:LRTTFD>2.0.CO;2.

Spence, G.D., Hyndman, R.D., Davis, E.E., and Yorath, C.J., 1991, Seismic structure of the northern Cascadia accretionary prism: Evidence from new multichannel seismic reflection data, *in* Meissner, R., Brown, L., Dürbaum, H.-J., Franke, W., Fuchs, K., and Seifert, F., eds., Continental Lithosphere: Deep Seismic Reflections. American Geophysical Union Geodynamics Series 22, p. 257–263.

Stone, J.O., 2000, Air pressure and cosmogenic isotope production. Journal of Geophysical Research, v. 105, p. 23,753–23,759, doi:10.1029/2000JB900181.

Storti, F., and McClay, K., 1995, Influence of syntectonic sedimentation on thrust wedges in analogue models. Geology, v. 23, p. 999–1002, doi:10.1130/0091-7613 (1995)023<0999:IOSSOT>2.3.CO;2.

Synal, H.-A., Stocker, M., and Suter, M., 2007, MICADAS: A new compact radiocarbon AMS system. Nuclear Instruments & Methods in Physics Research: Section B, Beam Interactions with Materials and Atoms, v. 259, p. 7–13.

Tucker, G.E., and Whipple, K.X., 2002, Topographic outcomes predicted by stream erosion models: Sensitivity analysis and intermodel comparison. Journal of Geophysical Research, v. 107, 2179, doi:10.1029 /2001JB000162.

van den Berg, M.W., and van Hoof, T., 2001, The Maas terrace sequence at Maastricht, SE Netherlands: Evidence for 200 m of late Neogene and Quaternary surface uplift, *in* Maddy, D., Macklin, M.G., and Woodward, J.C., eds., River Basin Sediment Systems: Archives of Environmental Change. Lisse, Netherlands, Balkema, p. 45–86.

van Zeist, W., and Wright, H.E., 1963, Preliminary pollen studies at Lake Zeribar, Zagros Mountains, southwestern Iran. Science, v. 140, p. 65–67, doi:10.1126 /science.140.3562.65.

Vassallo, R., Ritz, J.-F., and Carretier, S., 2011, Control of geomorphic processes on ^{10}Be concentrations in individual clasts: Complexity of the exposure history in Gobi-Altay range (Mongolia). Geomorphology, v. 135, p. 35–47, doi:10.1016/j.geomorph.2011.07.023.

Vernant, P., Nilforoushan, F., Hatzfeld, D., Abbassi, M.R., Vigny, C., Masson, F., Nankali, H., Martinod, J., Ashtiani, A., Bayer, R., Tavakoli, F., and Chéry, J., 2004, Present-day crustal deformation and plate kinematics in the Middle East constrained by GPS measurements in Iran and northern Oman. Geophysical Journal International, v. 157, p. 381–398, doi:10.1111 /j.1365-246X.2004.02222.x.

Vita-Finzi, C., 1969, The Mediterranean Valleys: Geological Changes in Historical Times. London, Cambridge University Press.

Vita-Finzi, C., 1975, Quaternary deposits in the Iranian Makran. The Geographical Journal, v. 141, p. 415–420, doi:10.2307/1796475.

Walker, R.T., and Fattahi, M., 2011, A framework of Holocene and Late Pleistocene environmental change in eastern Iran inferred from the dating of periods of alluvial fan abandonment, river terracing, and lake deposition. Quaternary Science Reviews, v. 30, p. 1256–1271, doi:10.1016/j.quascirev.2011.03.004.

Wegmann, K.W., and Pazzaglia, F.J., 2009, Late Quaternary fluvial terraces of the Romagna and Marche Apennines, Italy: Climatic, lithologic, and tectonic controls on terrace genesis in an active orogen. Quaternary Science Reviews, v. 28, p. 137–165, doi:10.1016/j .quascirev.2008.10.006.

Westaway, R., 2002, The Quaternary evolution of the Gulf of Corinth, central Greece: Coupling between surface processes and flow in the lower continental crust. Tectonophysics, v. 348, p. 269–318.

Whipple, K.X., 2004, Bedrock rivers and the geomorphology of active orogens. Annual Review of Earth and Planetary Sciences, v. 32, p. 151–185, doi:10.1146 /annurev.earth.32.101802.120356.

Whipple, K.X., and Tucker, G.E., 1999, Dynamics of the stream-power river incision model: Implications for height limits of mountain ranges, landscape response timescales, and research needs. Journal of Geophysical Research, v. 104, p. 17,661–17,674, doi:10.1029 /1999JB900120.

Whipple, K.X., Snyder, N.P., and Dollenmayer, K., 2000, Rates and processes of bedrock incision by the Upper Ukak River since the 1912 Novarupta ash flow in the Valley of Ten Thousand Smokes, Alaska. Geology, v. 28, p. 835–838, doi:10.1130/0091-7613(2000)28 <835:RAPOBI>2.0.CO;2.

Willett, S.D., Fisher, D., Fuller, C., En-Chao, Y., and Chia-Yu, L., 2003, Erosion rates and orogenic-wedge kinematics in Taiwan inferred from fission-track thermochronometry. Geology, v. 31, p. 945–948, doi:10.1130/G19702.1.

Wobus, C., Whipple, K.X., Kirby, E., Snyder, N., Johnson, J., Spyropolou, K., Crosby, B., and Sheehan, D., 2006, Tectonics from topography: Procedures, promise, and pitfalls, *in* Willett, S.D., Hovius, N., Brandon, M.T., and Fisher, D.M., eds., Tectonics, Climate, and Landscape Evolution. Geological Society of America Special Paper 398, p. 55–74, doi:10.1130/2006.2398(04).

Wong, I.G., 2005, Low potential for large intraslab earthquakes in the central Cascadia subduction zone. Bulletin of the Seismological Society of America, v. 95, p. 1880–1902, doi:10.1785/0120040132.

Science Editor: Christian Koeberl
Associate Editor: Jeffrey Clark

Manuscript Received 19 December 2013
Revised Manuscript Received 4 August 2014
Manuscript Accepted 5 September 2014

Printed in the USA